5 Undulators for SASE and spontaneous emission

5.1 Overview

5.1.1 Principles of XFEL operation

The free-electron laser (FEL) consists of a relativistic electron beam and a radiation field interacting with each other while propagating through an undulator **[5-1, 5-2]**. The FEL, despite its name, is not actually a laser; it is more closely related to vacuum-tube devices. As with vacuum-tube devices, FEL devices can be divided in two classes: amplifiers and oscillators. The FEL amplifier is a single-pass device. The FEL oscillator can be considered as an FEL amplifier with a feedback. For an FEL oscillator in the optical wavelength range, the feedback is carried out by means of an optical resonator. FELs based on the oscillator principle reach a limit at ultraviolet energies, primarily because of mirror limitations. Free-electron lasing at energies higher than the ultraviolet can be achieved with a single-pass, high-gain FEL amplifier operating in the Self-Amplified Spontaneous Emission (SASE) mode. These are the devices we refer to as X-Ray FELs (XFELs) in the following sections.

In an XFEL, radiation is produced by the electron beam during a single-pass of the undulator **[5-3 – 5-6]**. The amplification process starts from shot noise in the electron beam. During the amplification process a powerful, coherent radiation is produced having a narrow band near the resonance wavelength:

$$\lambda = \frac{\lambda_u}{2\gamma^2}\left(1 + K_{rms}^2\right)$$

<div align="right">(5.1)</div>

where λ_u is the undulator period, $K_{rms}=eH_{rms}\lambda_u/2\pi m_e c^2$ is the undulator parameter, H_{rms} is the rms-value of the undulator field, $\gamma=E/m_e c^2$ is the relativistic factor, E is the energy of the electron, -e and m_e are the charge and the mass of the electron, respectively, and c is the velocity of light. CGS units are used in this section therefore giving H=B with the relation between rms- and maximum values of $(H_{rms}, B_{rms})=(H_{max}, B_{max})/\alpha$ with $\alpha=1$ for helical magnetic field distribution and $\alpha=2^{1/2}$ for planar sinusoidal (linear) magnetic field distribution.

The electromagnetic wave amplification in the undulator refers to a class of self-consistency problems. It can be separated into two parts: a) solution of the dynamical problem, i.e. finding the motion of the particles under the action of the given electromagnetic fields; b) solution of the electrodynamics problem, i.e. finding the electromagnetic fields generated by a given distribution of charges and currents. To close the loop, the field equations and the equations of motion should be solved simultaneously. Nowadays,

FEL theory has reached a mature status allowing complete description of the FEL process. The optimisation process for the XFELs at the European XFEL Facility has been performed with a combination of analytical techniques **[5-7 – 5-14]**, and simulations with linear and non-linear steady state and time-dependent FEL simulation codes **[5-7, 5-13 – 5-19]**. Comparison of these simulations with experimental results obtained at the Free-electron LASer in Hamburg (FLASH) demonstrated very good agreement, which convinces us that the physical models and simulation tools developed adequately describe the XFEL process **[5-20 – 5-25]**.

5.1.2 Design criteria for the European XFEL

The scientific proposals for investigations using XFEL and spontaneous synchrotron radiation presented in Chapter 6 are based on the key properties of this radiation. Namely, on the ultrashort photon pulse duration of approximately 100 fs, on the high degree of coherence, on the outstanding peak brilliance, and last but not least, on the average brilliance **[5-26 – 5-28]**. In the design of the European XFEL Facility and its undulators the requirements with respect to photon energy range and tunability are important. The scientific case shows that most experiments which are not interested in particular resonances, will benefit from using photon energies close to 12.4 keV or slightly above. The design was, therefore, optimised to produce XFEL radiation at 12.4 keV simultaneously at two of the three XFEL undulators. These devices are called SASE 1 and SASE 2. In addition, the present design includes one XFEL for the soft x-ray range (SASE 3) and two undulators for spontaneous synchrotron radiation (U1, U2). SASE 3 corresponds to the demand for FEL radiation in the soft x-ray range and U1 and U2 provide ultrashort, highly coherent x-ray radiation in the 20 to 100 keV range for ultrashort time-scale physics and materials sciences investigations. A sketch of the different undulators and principal elements of the electron beam distribution can be found in Figure 5.1.1, and Table 5.1.1 lists all undulators and their design criteria.

In order to enable experiments over a continuous photon energy range up to 12.4 keV, SASE 2 is designed to be tunable in photon energy by changing the gap height. Tuning by changing the electron energy would be possible in principle, however, this change cannot be done very quickly except for a dynamic range of ± 1.5% (see Section 4.5) and it would affect the operation of all instruments. Tunability by gap variation has consequences for the saturation length (see Section 5.2.1). The tunability of SASE 2 has been set to the range 3.1 to 12.4 keV to limit both the total length and the number of x-ray optics. In contrast, SASE 1 is designed to operate at fixed photon energy of 12.4 keV. Due to the stringent requirements on the electron phase-space volume, XFEL undulators can be placed behind each other only on the condition that the second XFEL radiates at at least four times smaller photon energy. The SASE 3 undulator has been placed behind SASE 1 since the latter operates always at the highest photon energy. In contrast, spontaneously emitting undulators can be placed without problems behind XFELs. The two spontaneous emitting undulators use the spent electron beam of SASE 2. The undulators are planar, hybrid devices with a sinusoidal vertical field, apart from SASE 3 which is designed as an APPLE II device providing circular and linear polarised radiation. SASE 3 is constructed in this manner as there are currently no other means to efficiently generate circular polarised light in this energy region.
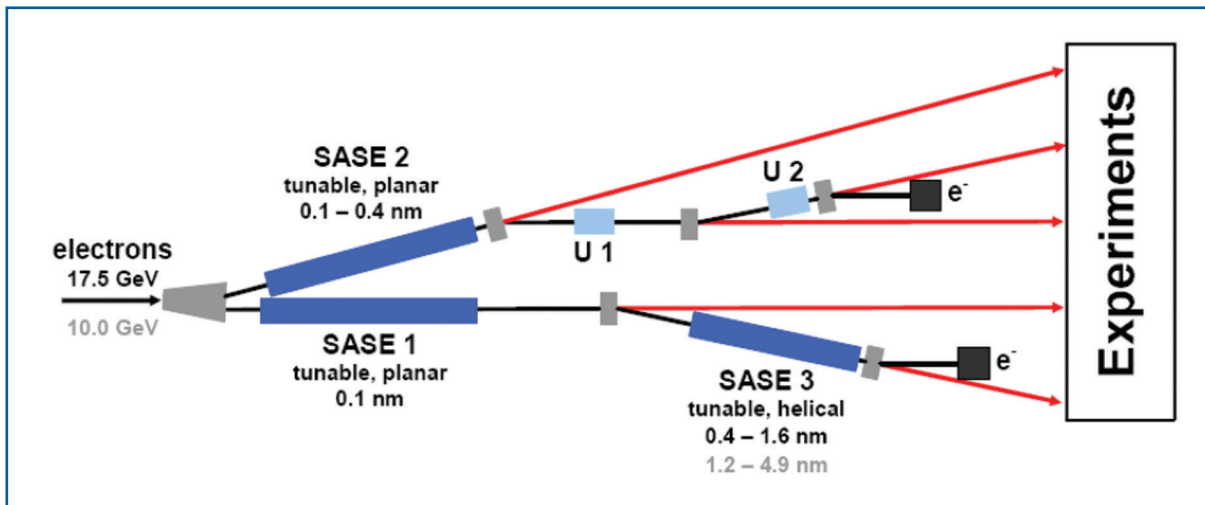
Figure 5.1.1 *Schematic overview of the electron beam distribution between accelerator and experimental hall. The two electron beamlines (black) include the five undulator systems for SASE FEL and spontaneous synchrotron radiation, which in turn feed five photon beamlines (red). The distance between the separation into two electron beamlines and the experimental hall is ~1300 m.*

	Photon energy [keV]	Polarisation	Tunability	Gap variation
SASE 1	12.4	Linear	No	Yes
SASE 2	3.1 – 12.4	Linear	Yes	Yes
SASE 3	0.8 – 3.1 (0.25 – 1.0)*	Circular/Linear	Yes	Yes
U1, U2	20 – 100	Linear	Yes	Yes

Table 5.1.1 *Design criteria for the five undulators of the European XFEL Facility. The photon energies correspond to an operating energy of the electron beam of 17.5 GeV. The asterisk denotes values for an electron energy of 10 GeV (see text).*

The European XFEL Facility should provide simultaneous operation of different beamlines with independent choice of photon energy. At a fixed energy of the electron beam of 17.5 GeV, independent tuning of the radiation wavelength is performed individually at each beamline by means of changing the undulator gap. In the case of SASE 3, a significant extension of the tunability could be achieved with an electron energy of 10 GeV. In addition, parameters for an additional XFEL for the range 0.2 – 0.8 keV at electron energy of 17.5 GeV are available [5-29].

Starting points for the optimisation of the XFEL sources are the design values for the photon energy ranges, the requirements for photon beam properties, the design parameters of the electron beam, and the restrictions provided by undulator technology. The applied design parameters for the electron beam are compiled in Table 5.1.2. The choice of undulator technology imposes certain restrictions on the optimisation process as well. The discussion of magnetic properties of the undulators is given in Section 5.4.

	Value	Unit
Electron energy	17.5	GeV
Bunch charge	1	nC
Peak current	5	kA
Bunch length (rms)	25	µm
Normalised emittance (rms)	1.4	mm mrad
Energy spread (rms)	1.5	MeV
Bunches per RF pulse	3000	
Repetition rate	10	Hz

Table 5.1.2 *Electron beam parameters used for the optimisation of the XFEL sources. The energy 17.5 GeV is already the result of an optimisation as is explained in Section 5.2.1 below.*

5.2   FEL radiation parameters

A zero-order estimation of the FEL characteristics is usually performed in the framework of the one-dimensional model in terms of the FEL parameter ρ_{1D} **[5-5]**:

$$\rho_{1D} = \frac{\lambda_u}{4\pi} \left[\frac{4\pi^2 j_o K_{rms}^2 A_{jj}^2}{I_A \lambda_u \gamma^3} \right]^{1/3} \tag{5.2}$$

Here j_0 is the beam current density, and $I_A = mc^3/e = 17$ kA. The coupling factor A_{jj} is equal to 1 for helical magnetic fields, and $A_{jj} = [J_0(Q)-J_1(Q)]$ for linear fields. Here J_n is the Bessel function of the first kind and $Q = K_{rms}^2/[2(1+K_{rms}^2)]$. Basic characteristics of the SASE FEL are simply estimated in terms of the parameter ρ_{1D} and the number of co-operating electrons $N_c = I/(e\rho_{1D}\omega)$ **[5-7, 5-13]**:

Field gain length: $\qquad L_g \approx \lambda_u/(4\pi\rho_{1D})$

Saturation length: $\qquad L_{sat} \approx 10 \times L_g$

Effective power of shot noise: $\qquad \dfrac{W_{sh}}{\rho_{1D} W_b} = \dfrac{3}{N_c\sqrt{\pi \ln N_c}}$,

Saturation efficiency: $\qquad \rho_{1D}$,

Power gain at saturation: $\qquad G = \dfrac{N_c}{3}\sqrt{\pi \ln N_c}$,

Spectrum bandwidth: $\qquad 2\rho_{1D}$,

Coherence time at saturation: $\qquad \tau_c = \dfrac{1}{\rho_{1D}\omega}\sqrt{\dfrac{\pi \ln N_c}{18}}$ $\qquad$ (5.3)

Undulators for SASE and spontaneous emission

Here W_b=EI/e is the electron beam power, and $\omega=2\pi c/\lambda$ is the frequency of the electromagnetic wave. Although useful for quick qualitative estimations of the parameter range, the one-dimensional approach does not provide reliable quantitative estimates and a complete three-dimensional theory of the FEL amplifier must be used instead.

We assume nearly uniform focusing of the electron beam in the undulator, by using the axisymmetric model of the electron beam to optimise the XFELs (the validity of this approach has been checked later with the actual focusing structure, using a non-axisymmetric model). It is assumed that the transverse distribution function of the electron beam is Gaussian, so that the rms transverse size of the matched beam is $\sigma=(\varepsilon\beta)^{1/2}$, where $\varepsilon=\varepsilon_n/\beta$ is the rms beam emittance and β is the focusing beta-function. The energy spread is also assumed to be Gaussian with rms spread σ_E, and the electron beam has a Gaussian longitudinal profile with rms bunch length σ_z.

In the framework of the three-dimensional theory, the operation of the FEL amplifier is described by the following parameters: the gain parameter Γ, the diffraction parameter B, the efficiency parameter ρ, the space charge parameter $\hat{\Lambda}_P^2$, the energy spread parameter $\hat{\Lambda}_T^2$, and the betatron motion parameter $\hat{k}_\beta$ [5-7, 5-12]:

$$\Gamma = \left[I\omega^2\theta_s^2 A_{jj}^2 / (I_A c^2 \gamma_z^2 \gamma)\right]^{1/2} \ , \quad B = 2\Gamma\sigma^2\omega/c \ , \quad \rho = c\gamma_z^2\Gamma/\omega \ ,$$

$$\hat{\Lambda}_T^2 = (\sigma/E)^2/\rho^2 \ , \qquad \hat{k}_\beta = 1/(\beta\Gamma) \ , \qquad \hat{\Lambda}_P^2 = 2c^2/(A_{jj}\theta_s\sigma\omega)^2 \ . \qquad (5.4)$$

Here I is the beam current, $\gamma_z^2=\gamma^2/(1+K_{rms}^2)$, and θ_s=K/γ. Note that the 1-D FEL parameter (see above) is $\rho_{1D}=\rho/B^{1/3}$. Typical values of parameters for 12.4 keV XFEL radiation are: Γ^{-1}~3 m, B~50-120, ρ~1.5×10^{-3}, $\hat{\Lambda}_P^2$ ~10^{-4}, $\hat{\Lambda}_T^2$ ~0.02, and $\hat{k}_\beta$ ~0.07. An important feature of the parameters space of XFEL is that the space charge field does not influence the FEL process significantly and optimisation of the FEL parameters can be performed by only taking into account diffraction effects, the energy spread in the electron beam and effects of betatron motion.

The amplification process in the FEL amplifier goes through two stages: linear and non-linear. The linear stage lasts over significant fraction of the undulator length (about 80%), and the main target for XFEL optimisation is the field gain length. In the linear high-gain limit the radiation emitted by the electron beam in the undulator can be represented as a set of modes:

$$E_x + iE_y = \int d\omega \exp[i\omega(z/c-t)] \sum_{n,k} A_{nk}(\omega)\, \Phi_{nk}(r,\omega) \exp[\,\Lambda_{nk}(\omega)z + in\phi] \qquad (5.5)$$

When amplification takes place, the mode configuration in the transverse plane remains unchanged, while the amplitude grows exponentially with the undulator length. Each mode is characterised by the eigenvalue $\Lambda_{nk}(\omega)$ and the field distribution, eigenfunction $\Phi_{nk}(r,\omega)$ in terms of transverse coordinates. At sufficient undulator length, the fundamental TEM$_{00}$ mode is the main contribution to the total radiation power. Thus, an important parameter for XFEL optimisation is the field gain length of the fundamental mode, L_g=1/Λ_{00}, which gives a good estimate for the expected length of the undulator needed to reach saturation, L_{sat}=10×L_g. Optimisation of the field gain length has been performed by

means of numerical solution of the corresponding eigenvalue equations taking into account all the effects (diffraction, energy spread and emittance) **[5-11, 5-12]**. The performance of modern computers allowed us to perform a complete study of the parameter space of XFEL (which in fact is 11-dimensional). From the practical point of view, it is important to find an absolute minimum of the gain length corresponding to the optimum focusing beta function. For this practically important case,0 the solution of the eigenvalue equation for the field gain length of the fundamental mode and the optimum beta function are rather accurately approximated by **[5-30]**:

$$L_g = 1.67 \left(\frac{I_A}{I} \right)^{1/2} \frac{(\varepsilon_n \lambda_u)^{5/6}}{\lambda^{2/3}} \frac{(1+K_{rms}^2)^{1/3}}{K_{rms} A_{JJ}} (1+\delta) \quad ,$$

$$\beta_{opt} = 11.2 \left(\frac{I_A}{I} \right)^{1/2} \frac{\varepsilon_n^{3/2} \lambda_u^{1/2}}{\lambda K_{rms} A_{JJ}} (1+8\delta)^{-1/3} \quad ,$$

$$\delta = 131 \frac{I_A}{I} \frac{\varepsilon_n^{5/4}}{\lambda^{1/8} \lambda_u^{9/8}} \frac{\sigma_\gamma^2}{(K_{rms} A_{JJ})^2 (1+K_{rms}^2)^{1/8}} \quad , \tag{5.6}$$

for $\sigma_\gamma = \sigma_E / m_e c^2$. Equation (5.6) demonstrates the power of analytical techniques providing a clear interdependence of physical parameters defining operation of the XFEL.

Quantum fluctuations of incoherent undulator radiation are a complicating factor for the optimisation of XFEL parameters. When the electron beam moves in the undulator it also emits incoherent radiation. The mean energy loss of each electron by incoherent radiation is given by:

$$dE/dz = 2r_e^2 \gamma^2 H(z)^2 / 3 \tag{5.7}$$

where $r_e = e^2 / m_e c^2$ is the classical radius of the electron. When the relative energy loss of the electron $\Delta E_{SR}/E$ becomes comparable with the FEL bandwidth $\rho B^{-1/3}$, the undulator has to be tapered in order to compensate for this effect and maintain the resonance condition. This tapering is also required due to wake field effects (see Section 4.4.5).

A fundamental limit on the minimal achievable wavelength is imposed by the growth of the uncorrelated energy spread in the electron beam due to the quantum fluctuations of undulator radiation **[5-4, 5-30, 5-31]**. The rate of the energy diffusion is given by **[5-32]**:

$$\frac{d\sigma_\gamma^2}{dz} = \frac{14}{15} \lambda^2 r_e \gamma^4 \kappa_u^2 K_{rms}^2 F(K_{rms}) \tag{5.8}$$

where $\lambda_c = h/mc$ is the Compton wavelength, h is Planck constant, $\kappa_u = 2\pi/\lambda_u$, and

$$F(K) = 1.42 K_{rms} + (1+1.50 K_{rms} + 0.95 K_{rms}^2)^{-1} \quad \text{for a helical field,}$$

$$F(K) = 1.70 K_{rms} + (1+1.88 K_{rms} + 0.80 K_{rms}^2)^{-1} \quad \text{for a linear field.} \tag{5.9}$$

The effect of quantum energy diffusion grows drastically with the energy and imposes a severe limitation on the achievement of very short wavelengths [5-30]:

$$\lambda_{min}^{q}[nm] = \frac{0.4\varepsilon_n[\mu rad]}{I^{3/5}[kA]L_{tot}^{2/5}[m]} \quad .$$

(5.10)

The next step in optimisation of the XFEL parameters is the solution of the initial-value problem, i.e. the calculation of the coefficients $A_{nk}(\omega)$ appearing in (5.5). This has been done by means of a technique reported in [5-8, 5-10, 5-14]. At this stage we calculate the degree of transverse coherence of the radiation from the SASE FEL [5-14, 5-32]. Calculations show that the degree of transverse coherence of the output radiation at the end of the linear regime is high for all XFELs of the European XFEL Facility.

The final stage of XFEL calculations is the simulation of the FEL process with non-linear simulation codes. We started with the steady-state simulation code FS2R [5-15] and Genesis 1.3 [5-19] being run in the steady-state mode using as input signal the effective power of the shot noise obtained from the solution of the initial-value problem. Final calculations have been performed with the three-dimensional, time-dependent simulation code FAST [5-18]. Final parameters for the XFEL sources have been checked with dedicated runs of the FAST code performing direct simulation of the FEL process for the total number of electrons in the beam. The results have been used for the compilation of Table 5.2.2 of XFEL parameters.

5.2.1   Defining undulator parameters

The choice of undulator parameters was based on global optimisation of the parameter space given by (5.6) with additional constraints defined by quantum fluctuations of incoherent radiation (5.8) and the interdependence of undulator parameters defined by state-of-the-art technology. Optimised parameters of the undulators are presented in Table 5.2.1. The choice of the undulator gap and the nominal electron energy is a compromise between the requirements to limit the total undulator length and to preserve the high quality of the XFEL radiation. Figure 5.2.1 shows the dependence of the saturation length on the electron energy for XFEL optimised for 0.1 nm wavelength. One can see that there is definite tendency to shorten the saturation length by reduction of the undulator gap. The optimum electron energy is reduced as well. Reduction of the undulator gap from 10 mm to 6 mm has a benefit in reduction of the saturation length by about 30%. On the other hand, the negative effect of the gap reduction is an increased strength of the wake fields. Although these wake fields are not completely fatal for XFEL operation, their presence significantly complicates the tuning of the machine and results in significant reduction of the parameter space in terms of bunch charge and pulse length. Our studies show that an undulator gap of 10 mm is a value corresponding to tolerable wake fields, acting as a perturbation only (see Section 4.4.5.2). As for the electron energy, the benefit in cost reduction seems to be attractive. However, there exists a severe obstacle: reduction of the electron energy below a certain value leads to significant reduction in the degree of transverse coherence of the radiation for SASE FEL operating at the minimum wavelength around 0.1 nm. The figure of merit defining the degree of transverse coherence is the diffraction parameter B. When the diffraction parameter is small, the gain of the fundamental

mode significantly exceeds the gain of higher modes **[5-7]**. In this case the degree of transverse coherence is limited by the effect of finite spectral width only, but it remains relatively high **[5-14, 5-33]**. At large values of the diffraction parameter, the gain for all modes becomes comparable, and the, mode selection process (5.5) is suppressed. As a result, the degree of transverse coherence of the radiation falls dramatically. Figure 5.2.1 shows the dependence of the diffraction parameter B versus energy for an optimised XFEL. Note that this dependence is universal and does not depend on the undulator gap. For optimised parameters of the FEL amplifier the diffraction parameter scales strongly with energy as $1/E^{5/2}$. At the operating energy of the European XFEL of 17.5 GeV, the value of the diffraction parameter for SASE 1 is about 120, and the degree of transverse coherence of the radiation is about 80%. Operation at lower energy leads to drastic reduction of the degree of transverse coherence **[5-34]**. Figure 5.2.2 shows the simulated saturation lengths for undulators SASE 1 to SASE 3 for the electron energy 17.5 GeV as a function of the wavelength of XFEL radiation.

	λ [nm]	λ_u [mm]	g [mm]	B_{max} [T]	K	β [m]	L_{sat} [m]
SASE 1	0.1	35.6	10	1.0	3.3	32	133
SASE 2	0.1	47.9	19	0.63	2.8	45	174
	0.4		10	1.37	6.1	15	72
SASE 3	0.4	80.0	23	0.44	3.3	15	81
	1.6		10	0.91	6.8	15	50
	4.9		10	0.91	6.8	15	45

Table 5.2.1   *Undulator parameters as the result of optimisation.*

Detailed calculations of the output parameters of the radiation (temporal and spectral structure, statistical properties) have been performed using the time-dependent simulation code FAST **[5-18]** and taking into account all important physical effects: diffraction, slippage, energy spread and emittance effects. Final numbers have been checked by means of direct simulation of the FEL process with the actual number of electrons using a parallel version of the code FAST operating on a multi-processor computer. Parameters of the radiation from XFEL sources are compiled in Table 5.2.2, and Figures 5.2.3 and 5.2.4 illustrate the radiation properties for SASE 1 operating at a photon energy of 12.4 keV.
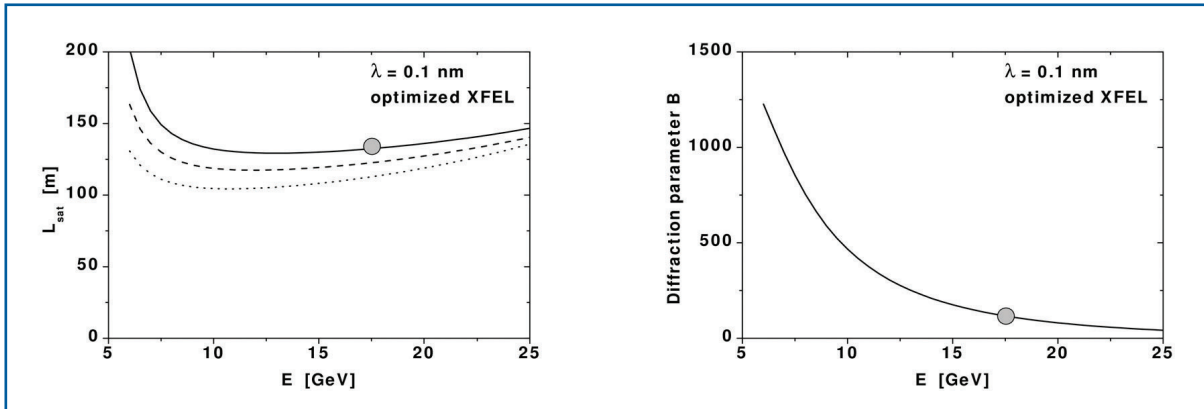
Figure 5.2.1 Left: Saturation length of an XFEL optimised for operation at 0.1 nm. Solid, dashed, and dotted lines correspond to undulator gaps of 10, 8, and 6 mm, respectively. Right: Diffraction parameter B against energy for an optimised XFEL. Circles correspond to the operating point of the European XFEL.
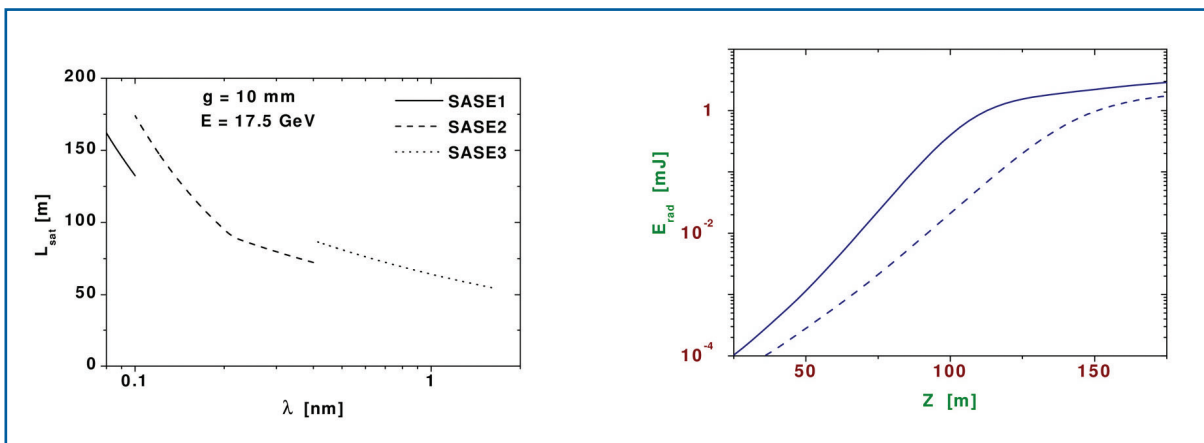
Figure 5.2.2 Saturation length against radiation wavelength for an electron energy of 17.5 GeV. The radiation wavelength is tuned by opening the undulator gap.
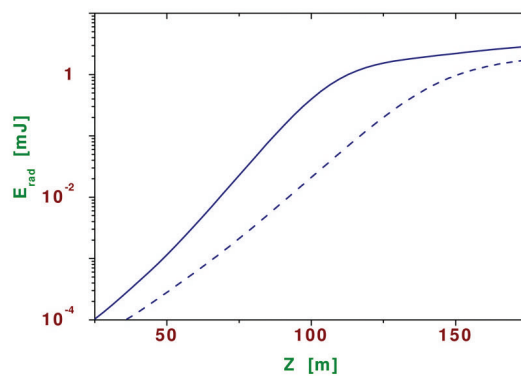
Figure 5.2.3 Average energy in the radiation pulse against magnetic undulator length for SASE 1 (solid line) and SASE 2 (dashed line) operating at 0.1 nm wavelength.
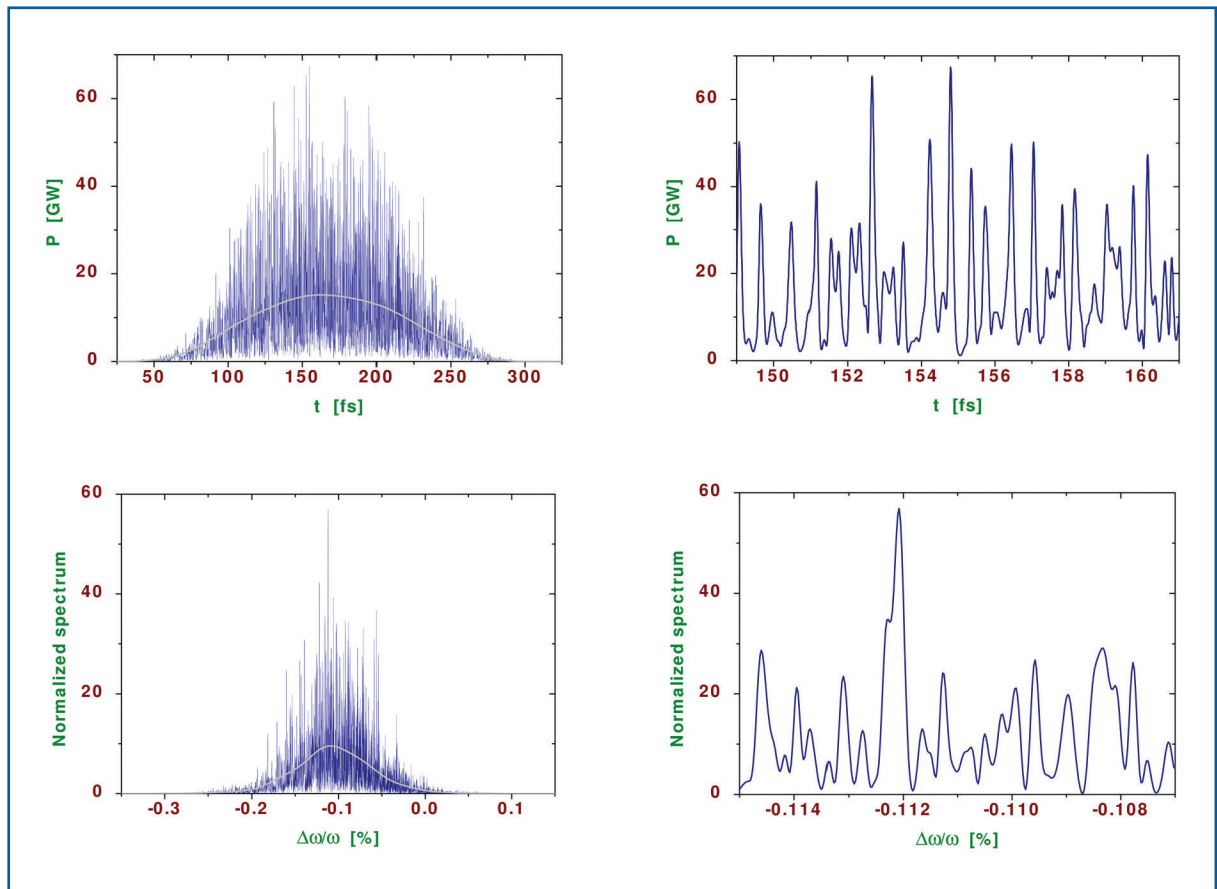
Figure 5.2.4 *Temporal (top) and spectral (bottom) structure for 12.4 keV XFEL radiation from SASE 1. Smooth lines indicate averaged profiles. Right side plots show enlarged view of the left plots. The magnetic undulator length is 130 m.*

	Unit	SASE 1		SASE 2		SASE 3	
Electron energy	GeV	17.5	17.5	17.5	17.5	17.5	10.0
Wavelength	nm	0.1	0.1	0.4	0.4	1.6	4.9
Photon energy	keV	12.4	12.4	3.1	3.1	0.8	0.25
Peak power	GW	20	20	80	80	130	150
Average power	W	65	65	260	260	420	490
Photon beam size (FWHM)	µm	70	85	55	60	70	90
Photon beam divergence (FWHM)	µrad	1	0.84	3.4	3.4	11.4	18
Coherence time	fs	0.2	0.22	0.38	0.34	0.88	1.4
Spectral bandwidth	%	0.08	0.08	0.18	0.2	0.3	0.65
Pulse duration	fs	100	100	100	100	100	100
Photons per pulse	#	10^{12}	10^{12}	1.6×10^{13}	1.6×10^{13}	1.0×10^{14}	3.7×10^{14}
Average flux	#/s	3.0×10^{16}	3.0×10^{16}	4.8×10^{17}	4.8×10^{17}	3.1×10^{18}	1.1×10^{19}
Peak brilliance	B	5.0×10^{33}	5.0×10^{33}	2.2×10^{33}	2.0×10^{33}	5.0×10^{32}	1.0×10^{32}
Average brilliance	B	1.6×10^{25}	1.6×10^{25}	6.5×10^{24}	5.9×10^{24}	1.4×10^{24}	2.8×10^{23}

Table 5.2.2 *XFEL radiation parameters for SASE 1 – SASE 3 as the result of simulations. Brilliance B is given in units of photons/0.1%bw/s/mm^2/mrad^2.*

5.2.2 Radiation parameters of SASE 3

SASE 3 uses the spent electron beam coming from SASE 1. Due to the SASE FEL process in SASE 1, the energy spread of the electron beam increases and is about 8 MeV at the entrance of SASE 3. The XFEL radiation parameters in Table 5.2.2 have been calculated for these parameters, and the saturation length is about 80 m at the radiation wavelength 0.4 nm. In this case the amplification process in SASE 1 is suppressed, e.g. by electron beam manipulation and the energy spread at the entrance of SASE 3 reduces to about 3 MeV. This value corresponds to the initial energy spread plus energy diffusion due to quantum fluctuations of the spontaneous radiation in the SASE 1 undulator. As can be seen in Figure 5.2.5, the saturation length reduces in this case from 80 to 70 m. The relative difference of the energy in the radiation pulse at the project length of SASE 3 (110 m) is about 20% for the cases of SASE 1 on/off.
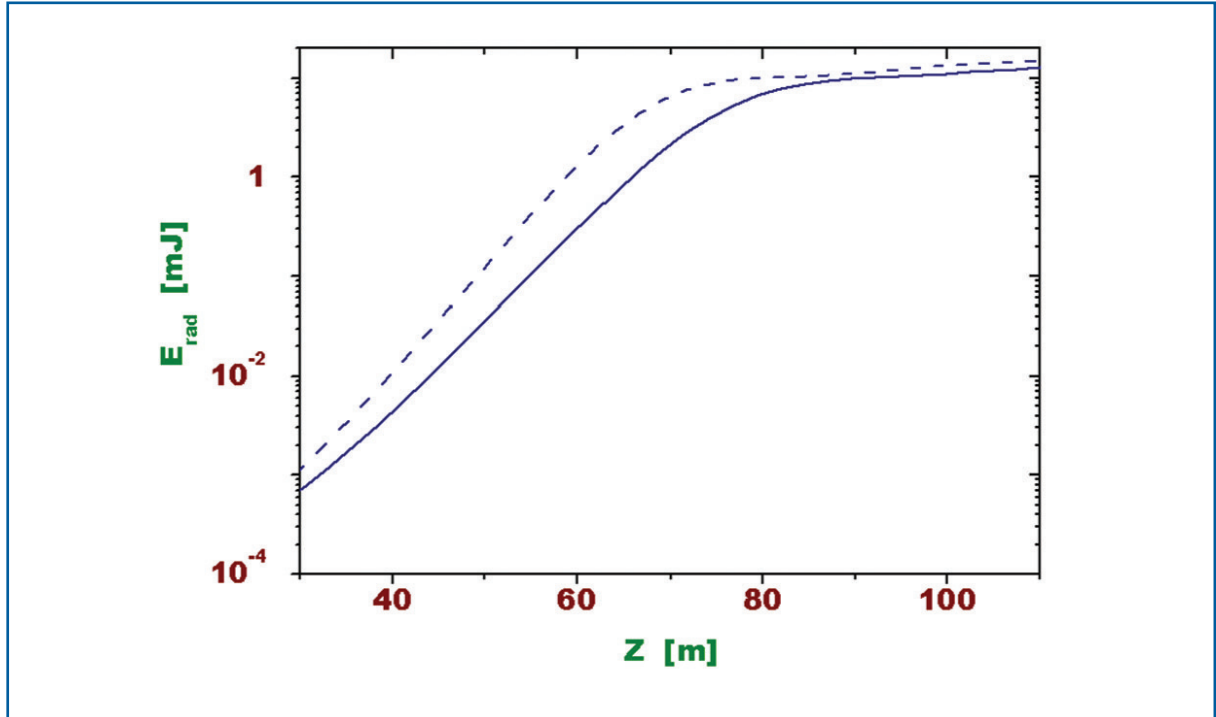
Figure 5.2.5 *Average energy in the radiation pulse against magnetic undulator length for SASE 3 operating at 0.4 nm wavelength. Solid and dashed lines correspond to the case of SASE 1 on/off, respectively.*

5.2.3 Statistical properties of the radiation

The radiation from SASE FEL operating in the linear regime possesses the typical properties of completely chaotic polarised light **[5-7, 5-13]**. Shot noise in the electron beam is a Gaussian random process; the FEL amplifier, operating in the linear regime, can be considered as a linear filter, which does not change statistics. As a result, radiation is also a Gaussian random process. In this case, the probability distribution of the instantaneous radiation power should be the negative exponential distribution (the notion of instantaneous power refers to a certain moment of time and a point in space, considered over an ensemble of pulses). Also, the finite-time integrals of the instantaneous power (energy in the radiation pulse) and the integrated spectral density (measured after the monochromator) should fluctuate in accordance with the gamma distribution **[5-7, 5-13]**:

$$P(W) = \frac{M^M}{G(M)} \left(\frac{W}{\langle W \rangle} \right)^{M-1} \frac{1}{\langle W \rangle} \exp\left(-M \frac{W}{\langle W \rangle} \right) \quad , \tag{5.11}$$

where $\Gamma(M)$ is the gamma function, $M = 1/\sigma_w^2$, and $\sigma_w = (\langle (W - \langle W \rangle)^2 \rangle)^{1/2}$. The parameter M can be interpreted as the average number of "degrees of freedom" or "modes" in the radiation pulse. Fluctuations reach maximum value at the end of the linear regime. A zero-order estimate for the number of longitudinal modes is $M = \sigma_z/(c\tau_c)$ with τ_c given by (5.3).

When approaching the saturation point, the statistical properties of the radiation change drastically on a scale of one field gain length **[5-7, 5-13, 5-33, 5-34]**. One useful property of the non-linear regime is the reduction of fluctuations of the radiation energy by about a factor of two with respect to the linear regime. Sensitivity of the radiation pulse energy with respect to jitters of machine parameters is reduced as well. Radiation power in the non-linear regime continues to grow due to the growth of sidebands in the non-linear media. As a result, spectrum broadening occurs. The spectral brightness and the degree of transverse coherence reduce as well. Maximum brightness of the radiation occurs at the undulator length of about ten field gain lengths.

5.2.4   Higher harmonics

Radiation of the electron beam in the planar undulator contains a rich harmonic spectrum. This refers to both incoherent and coherent radiation **[5-35 – 5-47]**. The fraction of higher harmonic content is very important for users planning experiments at the European XFEL. On the one hand, higher harmonics constitute a rather harmful background for some classes of experiments; on the other, higher harmonic radiation can significantly extend the operating band of the user facility.

A comprehensive study of the statistical properties of the odd harmonic radiation from SASE FEL has been performed in **[5-46]**, with the time-dependent simulation code FAST **[5-7, 5-18]** upgraded for simulation of non-linear harmonic generation. Application of similarity techniques allowed the derivation of universal formulae for the contribution of the odd harmonics to the total power of SASE FEL operating at saturation. In fact, this contribution is a universal function of the undulator parameter K and the longitudinal velocity spread parameter. For the European XFEL, simulations predict that the relative contribution to the total power of the third and the fifth harmonic is about 1% and 0.03%, respectively. Contribution of higher odd harmonics is at the level of spontaneous emission.

General statistical properties of the odd harmonics of the SASE FEL operating in saturation are as follows. The power of higher harmonics is subject to larger fluctuations than that of the fundamental one. Probability distributions of the instantaneous power of higher harmonics are close to the negative exponential distribution. The coherence time at saturation falls in inverse proportion to the harmonic number, and the relative spectral bandwidth remains constant with harmonic number.

There exists also a mechanism for non-linear generation of the second harmonic **[5-47]**. The contribution of the second harmonic to the total radiation power strongly depends on the value of the diffraction parameter B. Contribution of the second harmonic is expected to be about a fraction of a percent for SASE 3 operating at the wavelength around 1.6 nm, and is practically negligible for SASE 1 operating at 0.1 nm wavelength.

5.3　Spontaneous synchrotron radiation

The layout of the XFEL places two long undulators for spontaneous emission behind SASE 2. Although the electron beam performance is degraded by the SASE process, the beam still has a high quality compared to storage rings. Therefore, the minimum undulator gap can be reduced to 6 mm. Due to the small magnetic gap, high fields and consequently large K-values are possible. On axis, the spectrum consists of the well-known peaks of the odd harmonics and the design of the undulators allow for first harmonics in the hard x-ray regime. Furthermore, gap tuning allows coverage of the photon energy range up to nearly 100 keV using first and third harmonic radiation. Of course, the brilliance of spontaneous radiation is several orders of magnitude lower than that of FEL radiation, but its spectral range, time structure with ultrashort pulse durations of the order of <200 fs, and the high degree of coherence makes this radiation very interesting for a variety of experiments [see e.g. **5-48, 5-49**].

5.3.1　Undulator parameters

The U1 and U2 undulators will be realised in a similar fashion as the FEL undulators. Due to the length and the small gap the electron beam optics requires a FODO lattice inside the undulator sections the same as for the FEL undulators. The undulators are, therefore, designed to be built out of ten 5 m long segments with 1.1 m intersections between segments. Their magnetic length should be 50 m in order to increase the photon flux. Table 5.3.1 gives the parameters for the U1 and U2 undulators for two gap values. The electron beam parameters given in Table 5.1.2 are also valid for the undulator sections if one includes an increased energy spread of 8 MeV. The beta function in the undulator sections is 15 m.

5.3.2　Spontaneous radiation parameters

There are no simulation tools available today which are able to calculate the spontaneous radiation from the proposed undulator. The complexity of the long undulators with intermediate electron beam focusing and the phase problem of the ten segments, do not allow us to use existing tools for calculation of the radiation for the full length of all segments, that is for the full number of nearly 2,000 periods. Since the number of periods is an important parameter that relates directly to radiation properties such as opening angle of radiation and bandwidth, we cannot make an exact prediction of the expected values. Instead, we will give an estimate for the radiation from an incoherent superposition of ten 5 m long segments. This is certainly a lower level approximation. From Table 5.3.2 one observes the radiation parameters for four photon energies. Using the fundamental line, the entire energy range from 20 to 90 keV is accessed with a reasonable variation of the magnetic gap (see also Table 5.3.1). The energy range 20-30 keV is very suitable for diffraction experiments in a classical configuration and for exploiting the time-structure or the coherence of the beam. The energy range from 60 to 90 keV, provided either through the fundamental or by third harmonics radiation, is of high interest to materials science studies, again exploiting the time-structure and the coherence properties. The differences between using fundamental or 3rd harmonic radiation are factors up to 3

in relative bandwidth and photon flux through an aperture. In Table 5.3.2. we consider only the parameters of the fundamental harmonics, having larger bandwidth and higher photon flux.This table indicates that the flux in photons/pulse will be almost constant over the entire photon energy range. At the same time, the bandwidth narrows by one order of magnitude, the pulse duration is three orders of magnitude shorter, and the coherence improves when comparing it to storage ring sources. Therefore, the increase in brilliance is quite important. The main difference is the angular acceptance. Whereas with synchrotron sources, relatively large angular openings can be accepted due to the proximity of the optical element to the source, here the beam has to be transported ~100 m before the first optical element can be placed into the beam path. Placing a 1×1 mm^2 aperture at this distance reduces the acceptance to ~1% of the SR case. Figure 5.3.1 shows spectra for spontaneous radiation through this aperture for different settings of the undulator.

	Unit	'Closed gap' $\rightarrow$ 'Opened gap'			
Magnetic gap	mm	6	7.5	11.3	16.1
Photon energy range first harmonic	keV	20.2	30.6	60.1	90.1
Photon energy range third harmonic	keV	60.6	92	-	-
Period length	mm	26	26	26	26
Number of periods per segment		192	192	192	192
Number of segments		10	10	10	10
Magnetic field	T	1.24	0.95	0.54	0.28
K- parameter	mm	3	2.3	1.3	0.7

Table 5.3.1   Parameters for U1 and U2 undulators for spontaneous radiation.

	Unit	U1/U2 spontaneous synchrotron radiation			
Photon energy	keV	20.2	30.6	60.1	90.1
Photon beam size (FWHM)	μm	24.5	24.5	24.5	24.5
Photon beam divergence (FWHM)	μrad	3.0	2.6	2.2	2.0
Pulse duration (FWHM)	fs	200	200	200	200
Spectral bandwidth (FWHM)	%	0.77	0.98	1.66	2.33
Coherence angle	μrad	0.25	0.16	0.08	0.05
Photons per pulse	#	1.1×10^9	1.7×10^9	2.5×10^9	1.9×10^9
Average flux	#/s	3.4×10^{13}	5.0×10^{13}	7.5×10^{13}	5.6×10^{13}
Peak brilliance	B	3.1×10^{27}	3.9×10^{27}	4.3×10^{27}	2.5×10^{27}
Average brilliance	B	1.8×10^{19}	2.3×10^{19}	2.6×10^{19}	1.5×10^{19}

Table 5.3.2   Radiation parameters for U1 and U2 radiation at four photon energies calculated using the SPECTRA code [5-50] for the electron beam parameters given in Table 5.1.2 and an increased energy spread of 8 MeV. Calculations have been performed for 9×9 μrad^2 angular acceptance. Brilliance is given in units of photons/0.1%bw/s/mm^2/mrad^2.

In order to estimate if gain due to coherent superposition plays an important role, we have compared the values for 20 keV radiation from an undulator with 5 m coherent superposition length to those obtained for 10 and 20 m long segments. Here, we assume complete phasing and neglect the intersections for electron beam optics. Table 5.3.3 indicates that the flux through an aperture, given in photons per pulse, does not change. The differences in bandwidth and divergence of the beam lead, however, to an increase of the brilliance. We, therefore, do not expect large deviations from our simulations for the spontaneously emitted radiation.
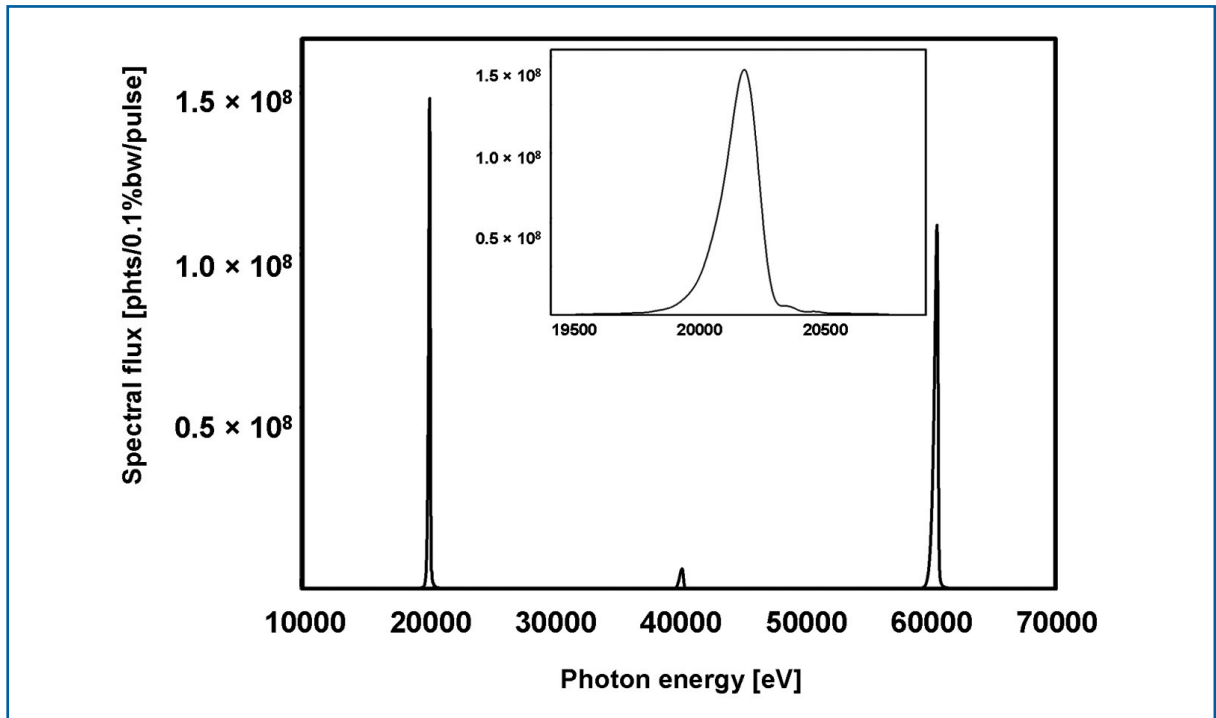
Figure 5.3.1 *Spectral flux through an angular aperture of 9×9 µrad² for spontaneous radiation from U1 undulator and a gap of 6 mm. The inset shows the fundamental line that has a bandwidth of 0.77%.*

	Unit	U1/U2 spontaneous synchrotron radiation		
Length of coherent segments	m	5	10	20
Photon beam size (FWHM)	µm	24.5	24.5	24.5
Photon beam divergence (FWHM)	µrad	3.0	2.4	2.0
Spectral bandwidth (FWHM)	%	0.77	0.64	0.57
Photons per pulse	#	1.1×10^9	1.1×10^9	1.1×10^9
Average flux	#/s	3.4×10^{13}	3.4×10^{13}	3.4×10^{13}
Peak brilliance	B	3.1×10^{27}	4.7×10^{27}	6.4×10^{27}
Average brilliance	B	1.8×10^{19}	2.8×10^{19}	3.8×10^{19}

Table 5.3.3 *Radiation parameters from U1/U2 for 20.2 keV calculated using the SPECTRA code [5-50] for the above parameters and assuming different lengths of the coherently radiating sections. Comparison is done for a total magnetic length of 50 m. Brilliance is given in units of photons/0.1%bw/s/mm²/mrad².*

5.4 Undulator systems

The undulator provides the periodic magnetic field which induces the FEL process. Compared to storage ring sources the undulators will be very long as the saturation length is of the order 100 m for x-ray radiation. It is clear that the electron beam requires focusing elements within the undulator section to preserve its lateral size. The electron beam parameters call for a "separate function" undulator, where the periodic magnetic field and the strong focusing are physically separated. The undulator system, thus, consists of undulator segments and separated strong focusing quadrupoles and phase adjusters, beam correctors, position monitors, etc. The European XFEL Facility includes three XFEL undulators and, in addition, two undulators for spontaneously emitted synchrotron radiation as shown in Figure 5.1.1. In the design of the undulators' systems, no fundamental difference is made between a FEL and a spontaneous undulator system. Therefore, in the following, no special distinction is made, and all undulator systems are treated in the same fashion. In Table 5.4.1 the parameters of the XFELs and spontaneous emitters are summarised.

The undulators described in this section are extremely demanding devices due to their length and their required accuracy. Many components of the undulators have to work together in a complex way. The most delicate and also most expensive items are the magnetic structures. But also the mechanical girders have extreme requirements to stability, precision, and reproducibility. Fortunately, there has been a tremendous development of insertion device technology since undulators have come into use as intense sources of synchrotron radiation 25 years ago. Considerable progress has been made in the design, construction and optimisation of these devices. There are well-established techniques to produce insertion devices with properties that are very close to perfect. Design and construction of undulator systems for the European XFEL will certainly take full advantage of these achievements.

5.4.1 Choice of undulator parameters

The basic concept for the layout and design of the undulator systems of the European XFEL is described in Section 5.1.2. For completeness Table 5.4.1 gives an overview of all five undulator systems, their spectral ranges and their parameters. According to this table a total of 116 segments are required for the XFEL. Substantial research and development (R&D) activities are needed to find an economic way to supply this quantity within time, quality and cost limits. These activities are described below. All undulators will be installed in tunnels with a diameter of 5.2 m in case of SASE 1 and SASE 2 and of 4.5 m in the cases of SASE 3, U1 and U2. In Figure 5.4.1 it is shown how a string of three segments would be placed inside the 5.2 m diameter tunnel. Tunnel infrastructure such as air conditioning, cable trays, piping, etc. is omitted. One cell consists of a 5 m long undulator segment and a 1.1 m long intersection. For the transport of undulator segments, a combination of a special transport vehicle similar to those used for magnet transport in accelerator tunnels with air cushions may be used. Fast transport in the XFEL tunnels over distances of several hundred metres at a speed of 2-3 km/h is possible in this way. At the insertion point the air cushions are used to move the segments in position. Then they are lowered

to stable floor plates. In the same fashion insertion devices are moved in DORIS III. If well optimised, an undulator segment may be exchanged in 1-2 hours.

	λ [nm]	λ_u [mm]	g [mm]	B_{max} [T]	K	β [m]	L_{sat}^{+} [m]	N_{tot}^{++} [m]	L_{tot}^{+++} [m]
SASE 1*	0.1	35.6	10	1.0	3.3	32	133	33	201.3
SASE 2*	0.1	48	19	0.63	2.8	46	174	42	256.2
	0.4		10	1.37	6.1	15	72		
SASE 3**	0.4	80.0	23	0.44	3.3	15	81	21	128.1
	1.6		10	0.91	6.8	15	50		
U1/U2***	0.06	26	6	1.24	3.0	15	-	10	61
	0.014		16	0.28	0.7	15	-		
						Total:		116	707.6

*   Planar hybrid undulator.
**   Apple II type helical undulator.
*** *Planar hybrid undulators for spontaneous radiation. Wavelength corresponds to first harmonic*
+   *Magnetic length without consideration of field errors.*
++   *Number of 5m undulator segments plus 20% contingency. Spontaneous emitters have 10 segments each.*
+++ *Total system length includes 1.1m long intersection after each undulator segment.*

Table 5.4.1   *Parameters of the undulator systems. The electron beam energy is 17.5 GeV.*
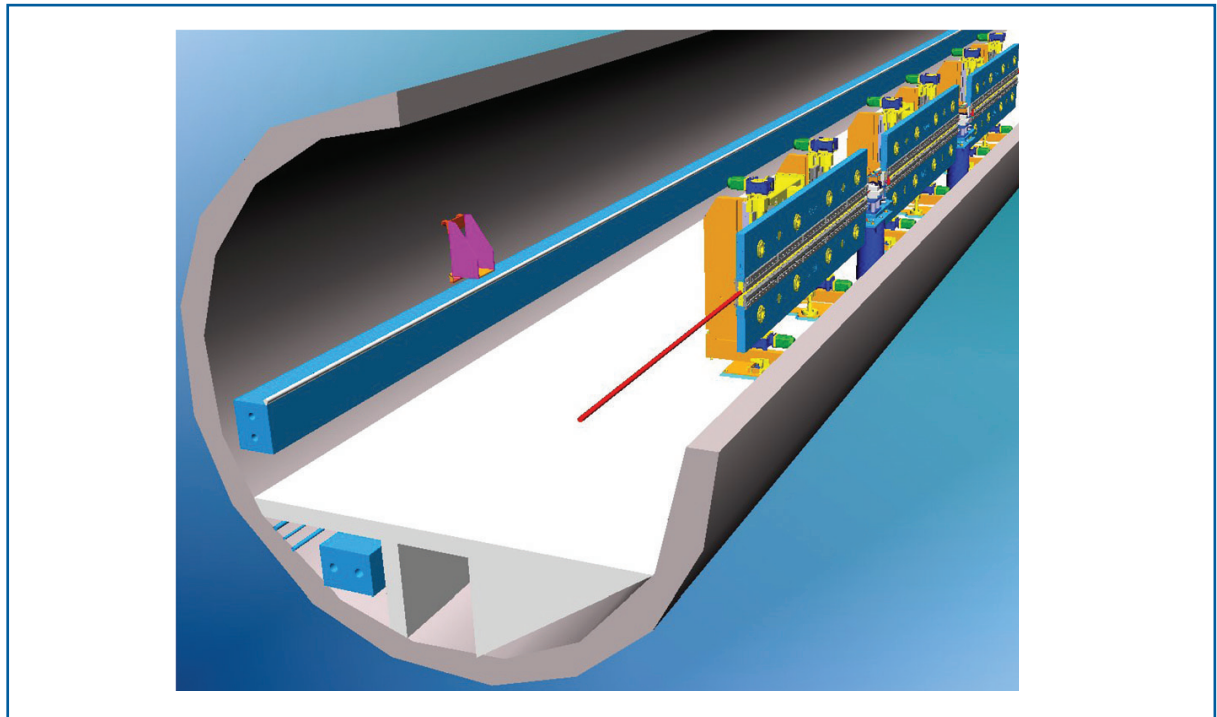
Figure 5.4.1   *A string of three cells of an undulator system is shown as it will be installed in a tunnel with a diameter of 5.2 m (SASE 1, SASE 2). Infrastructure such as air conditioning, cable trays, supply media are not included.*

5.4.1.1 Magnet technology

Undulators might be built using superconducting magnets, room-temperature electromagnets, or permanent magnets (PMs). These technologies were investigated and discussed in **[5-26, 5-51]**. In 2005, a workshop held at Deutsches Elektronen Synchrotron Laboratory (DESY) discussed the issue again and concluded that, at present, no alternative to PM technology for the large-scale use in undulator systems, such as the European XEL Facility is available. The hybrid design **[5-52]** uses NdFeB permanent magnets and soft Iron parts which concentrate the magnetic flux. For the hybrid design errors are mostly determined by the machined pole faces. In order to produce circularly polarised light, a modified planar pure PM structure was proposed by Sasaki **[5-53]**. With 25 years of development of undulator technology based on PMs, many techniques for error compensation have been developed. Technologically, all problems related to manufacturing of large numbers of undulator segments are solved:

- manufacturing techniques are well established, extensive experience exists;
- the magnet structures are planar, allowing for excellent access for magnetic field measurements and for the insertion of vacuum chambers;
- helical undulators can be built as planar devices as well;
- numerous high-precision magnetic field measuring techniques are available;
- control of field errors can be done using shims or field fine-tuning **[5-54 – 5-56]**.

The design proposal for the undulator systems for the European XFEL will, therefore, be based exclusively on PM technology. For the peak magnetic field the following dependence on material constants a_1, a_2, a_3, magnetic gap γ and undulator period λ_u is valid:

$$B_{max}(T) = a_1 \times \exp\left[a_2 \frac{g}{\lambda_u} + a_3 \left(\frac{g}{\lambda_u} \right)^2 \right] \quad . \tag{5.12}$$

For a state-of-the-art hybrid undulator made of NdFeB, a_1=3.694, a_2=-5.068, and a_3=1.520 are used. This assumption is valid for NdFeB for $0.1 < g/\lambda_u < 1.0$. The magnetic gap chosen for the XFEL and spontaneous emitters is 10 and 6 mm, respectively.

5.4.1.2 Radiation damage

Potential radiation damage of the PM material due to electron, neutron, and hard x-ray bombardment could endanger the required performance of the FEL undulators and, therefore, the performance of XFEL radiation. Until recently experience only existed for IDs in storage rings, where a very high transmission and, therefore, a very low loss rate is enforced by the requirement of long lifetime of the stored electron beam. Under normal operating conditions, no significant radiation damage has been observed **[5-57, 5-58]**. In contrast, not much was known about how PM undulators behave in the radiative environment of a high duty-cycle linac like the one proposed for the European XFEL. Here, the situation is completely different. Although the emittance and beam size are smaller than in storage rings, there might be a significant amount of beam halo and dark current far outside the phase-space covered by the transverse and longitudinal electron beam

emittance. A well-designed collimator system to protect the undulators from being hit by electrons is, therefore, essential. The collimator system is described in Section 4.7.1.2.

Recently, experience has been gained from the operation of the undulator system installed at the FLASH facility at DESY. At FLASH the radiation doses were continuously measured without interruption in a meticulous way over the whole operation time of the undulator at 15 positions equally spaced over the length of the device. Measurements made at the undulator system after de-installation showed that no damage could be detected within an accuracy of 2×10^{-4} after three years of operation and a maximum exposure of 12,000 Gy near the entrance **[5-59]**. An extrapolation to the XFEL based on these data resulted in even higher lifetimes. A coarse lifetime estimate for the magnet material can be made based on the results obtained at the TESLA Test Facility (TTF) facility with the following assumptions:

- we take the result of Okuda **[5-60]** who observed a 9% loss of demagnetisation of NdFeB material for an absorbed dose of 2.5 MGy after electron irradiation, equivalent to 1% for 0.28 MGy;

- the length of the radio frequency (RF) pulses needs to be considered since the radiation dose increases linearly with dark current;

- a factor of 50 accounts for the increased availability of the accelerator compared to the FLASH facility;

- we take the low dose levels at the undulator end for comparison, thus considering the first two segments as additional shielding elements.

Extrapolating thus gives an expected annual dose of 8,000 Gy for the undulators at the European XFEL. This is a worst case estimate and the real irradiation of the magnets will be less due to the following arguments:

- the electron accelerator of the European XFEL has phase-space as well as "energy" collimation. Dark current, therefore, cannot hit the undulator. In addition, the electron beam in the collimator does not point towards the undulator. This is discussed in detail in Section 4.7.1.2;

- the doses at FLASH are integrated over the whole previous life. They include runs with missteered electron beam, high dark current levels or non-optimum collimator adjustments as well. Such conditions contribute significantly to irradiation doses. In this project these unwanted beam conditions can be avoided thanks to the commissioning dump installed in front of the undulators;

- the gap of the FLASH undulator is fixed. In this project the gap can be opened for commissioning and beam optimisation. Thus, the irradiation at these operation modes will be avoided;

- online dosimeters and loss monitors will be installed **[5-61]** giving a clear signal, if the dose level inside the undulator region becomes too high.

The resulting worst case lifetime estimate for 1% demagnetisation is 35 years. This estimate does not include the above relieving arguments. As a result, NdFeB should be fully sufficient as undulator magnetic materials, and the radiation harder magnets samarium and cobalt will not be used. Nevertheless, fast exchange of undulator segments is desirable as a conservative fallback solution in case that radiation damage becomes a problem.

5.4.2   Basic tolerance requirements

The line width of FEL radiation is determined by the dimensionless Pierce parameter ρ_{1D} (5.2), which for an XFEL at 0.1 nm amounts to 3×10^{-4}. For the undulator system this means that the fundamental wavelength has to be tuned with an accuracy given by:

$$\frac{\Delta\lambda}{\lambda} \leq \rho \qquad . \tag{5.13}$$

The nature of the FEL process is such that, in order to have an effect on the radiated power, an error has to act over a power gain length, which for the XFEL is in the order of 10 m. Certainly, a conservative requirement would be for (5.13) to be valid for one undulator segment, which is only 5 m long. There are different error sources having an effect on the fundamental line: temperature via the temperature-dependent magnetisation coefficient of the magnet material, vertical alignment via the hyperbolic-cosine field distribution, gap and flatness errors via the exponential field dependence. If all error sources are equally weighted and using

$$\Delta\lambda = \left|\frac{\partial\lambda}{\partial B}\right| \sqrt{\Delta B_{Temp}^2 + \Delta B_{Gap}^2 + \Delta B_{Flat}^2} \tag{5.14}$$

one obtains the values given in Table 5.4.2.

Temperature stability (whole system)	ΔT	± 0.08	K
Alignment (each segment)	ΔY	± 100	µm
Gap accuracy (each segment)	Δg	± 1	µm
Flatness change of each segment under gap change	Δg	± 1	µm

Table 5.4.2   *Undulator systems tolerances.*

There are two consequences of these requirements:

- the whole undulator system must be in a very well controlled temperature environment. The impact of this requirement on the tunnel layout and air conditioning system will be discussed in Section 7.2.3;

- the geometric tolerances have a strong impact on the mechanical design and requirements on the control system. This will be addressed in the next section.

5.4.3 Undulator segments

The huge total length of the undulator section calls for standardisation and an economic design that is optimised for the production of large quantities. Several aspects play a role in long undulator systems for SASE FELs. The total length of an undulator system is much longer than the optimum β-function for largest FEL gain. External strong focusing is, therefore, needed to keep the β-function within limits acceptable for the FEL process. The undulator system will be separated into undulator segments and strong focusing quadrupoles. With the single exception that a second working point at 10 GeV electron energy could be established in order to enable access to the soft x-ray regime below 800 eV, the photon energy of the FEL and spontaneous radiation will be changed by gap tuning. This increases the saturation length and leads to a requirement for tunable phase shifters. It could also induce gap dependent field errors. Only four different types of magnet structures are needed for a total of 116 segments. In the design and construction one, therefore, should take advantage of the large numbers by using standardised components wherever possible. Items which will contain as many identical components as possible are:

- the gap separation drive systems, motion control components, motors, servos;

- girders;

- components inside the undulator interruptions, such as phase shifters, corrector magnets and their power supplies, quadrupole magnets, and beam position monitors (BPMs);

- control systems for gap motion and gap dependent excitation of coils, readout of BPMs, etc.;

- vacuum chambers and other vacuum equipment.

Instead of optimising the components for different undulators individually, they will be designed for the most demanding case. For example, mechanical gap separation drive systems and girders will be designed for maximum magnetic forces occurring at the most critical undulator and then adopted for all of them. Phase shifters should be designed to meet the phase shifting requirements at the longest wavelength. This standardisation policy leads to most economical solutions in terms of production, prototyping, operation and maintenance.

5.4.3.1 Support mechanics

A mechanical design has been worked out, which complies with the accuracy requirements given in the previous section and in addition takes care of boundary conditions specific to the XFEL project, such as tunnel cross-section, transport in the tunnels, exchangeability of undulator segments, fast alignment, escape routes and other safety issues. Since large numbers of devices are required, the effort concentrates on designing one standard system. Critical design parameters were chosen conservatively in order to reduce the risk in fulfilling design performances for each of the segments in an industrial production process.

Figures 5.4.2 and 5.4.3 give a front and rear view of a proposed standard undulator segment for the XFEL. It is flexible enough to accommodate different types of magnetic structures.
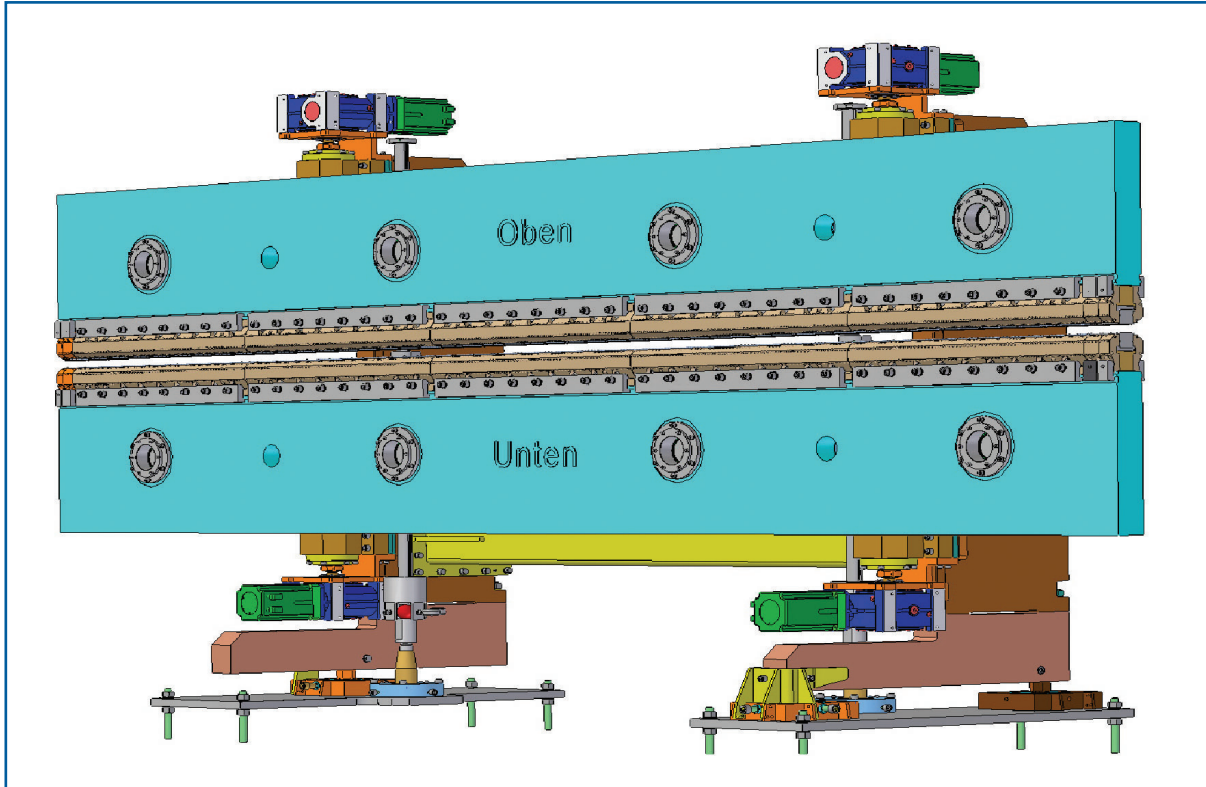

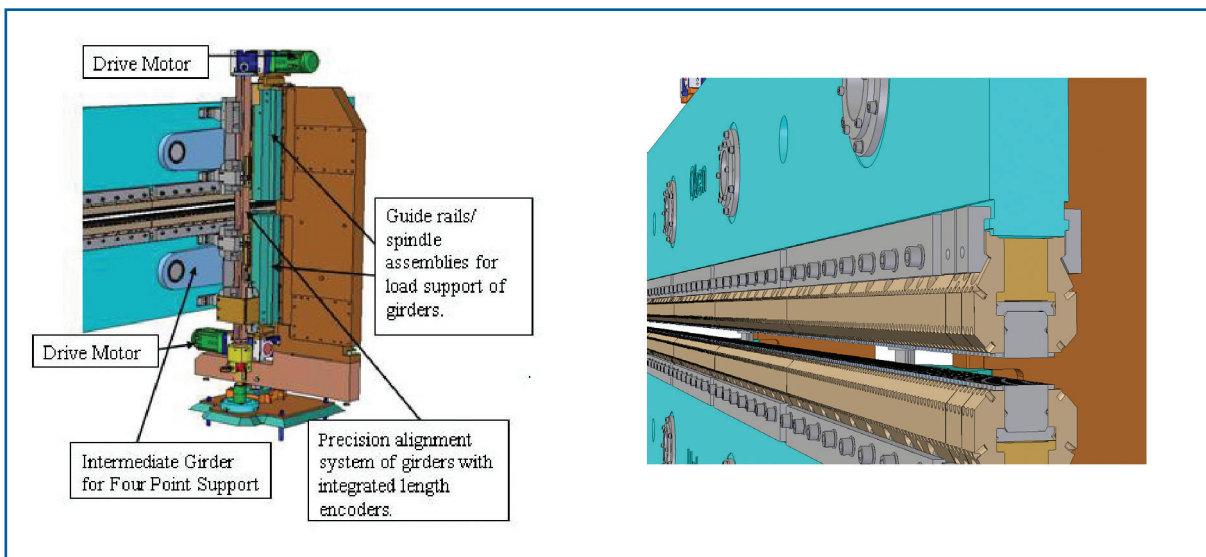**Figure 5.4.2**   *Front view of a 5 m long undulator segment.*

Figure 5.4.3   *Rear view showing details of the intermediate girder and the precision alignment system. The support frame has been suppressed to give a better view.*
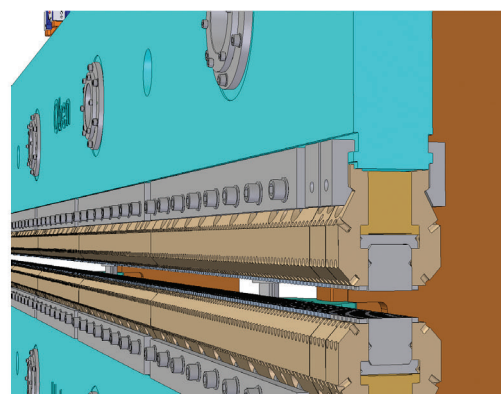
Figure 5.4.4   *Clamping principle of the magnetic structure on the girders.*

There are several points, which deserve being mentioned:

- the girders have a substantial rectangular cross section of 500 by 100 mm to minimise shear deformation, which, in the µm range, dominates over compressive deformation;

- in order to avoid bimetallic bending as a function of temperature on the µm level, the materials for girders and support structures need to be identical. Suitable stainless steel with magnetic permeability smaller than 1.02 (e.g. Type 1.4429) will be taken for magnetic and mechanical stability reasons;

- each girder is supported on four equidistant points as seen in Figure 5.4.2. This reduces the deformation under changing magnetic loads dramatically. Two auxiliary, intermediate girders are needed, which are seen in the rear view in Figure 5.4.3;

- there are four motors, one for each spindle. They are electronically synchronised by a suitable control system;

- the girders are connected to massive guideways and lead screws integrated in the support columns using spherical supports. In this way the magnetic forces are transmitted and a rotational degree of freedom is provided. The exact parallel alignment of top and bottom girder is achieved through a separate guiding system, using movers with preloaded roller bearings free of backlash. This is also shown in Figure 5.4.3. The guiding system also integrates the encoders needed for the high precision position feedback for the four drive motors. Although guiding forces on the guide rails are small, and only originate in residual friction in the supports, their sizes are quite substantial in order to guarantee parallel alignment with high precision.

5.4.3.2   Magnetic structures

The magnet structures are clamped onto the girders. This allows for a girder design which is independent of details of the magnet structure. This is illustrated in Figure 5.4.4. Identical materials are used for the girders and the non-magnetic support parts in order to avoid any bimetallic deformation as a function of temperature.

The mechanical design of the magnetic structure takes advantage of experience gained from the undulator system for the FLASH facility at DESY. Segments of 0.957 m length are used. One is shown in the left of Figure 5.4.5. In addition, end sections made in the same fashion are needed.
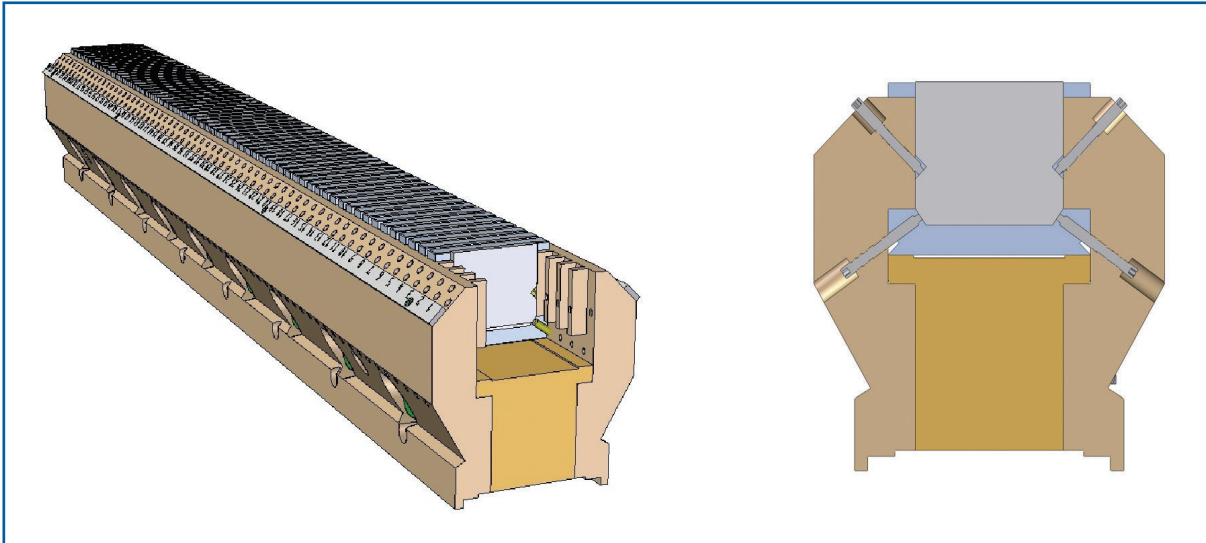
Figure 5.4.5 *Left: Assembly of one 0.957 m long magnet segment. The first magnets and poles are not inserted. A 5 m long device uses five segments plus compensation pieces built in exactly the same fashion. Right: Cut through a pole showing the height adjustment principle. The height of a pole can be adjusted by at least ± 0.3 mm and its tilt by about ± 1 mrad. The screws from below are used to lock the pole in position.*

As seen in Figure 5.4.5 there is a comb-like structure with pockets for the magnets and slits for the poles. Magnets and poles are pinned down using worm screws at approximately 45°, which act onto notches in the magnets and poles (compare Figure 5.4.5). For the poles this allows fine adjustment of the height. From the bottom there are counter-screws, which are used to lock a pole in position. The tolerances are chosen in such a way that the overall vertical position can be varied by at least ±0.3 mm and in addition, the tilt of the poles can be adjusted by ±1 mrad by using the right and left adjustment screws. Starting with an initial pole overhang of 0.5 mm the exact adjustment of the poles is done during magnetic measurements. Typical corrections are less than ±0.1 mm. They will be determined using measured magnetic field data and applying the method of "Field fine tuning by Pole Height Adjustment" **[5-56]**.

This method assigns measured field errors to pole height corrections for each pole. A high field quality can be obtained in this way.

5.4.3.3 Control system

There are several requirements on the control system in order to make full use of the capabilities of the undulator system. The control system:

- has to coordinate and synchronise the motion of the four motors of an undulator segment with high precision. The gap should be adjusted with an accuracy of less than 1μm. In addition, operational safety such as proper recognition of equipment failure, breaking of cables, loss of synchronisation, etc. has to be guaranteed;

- has to allow for synchronisation of additional components, for example current settings of corrector coils, gap values for phase shifter settings, etc. It should be possible to implement these corrections in a flexible manner;

- must be modular and easily extendable: It must provide control of the whole undulator system, i.e. synchronisation of many individual cells;

- should be designed for a life time of 15-20 years minimum;

- should be designed for high reliability and availability of components;

- makes use of industrial standards and components wherever possible.

A concept has been developed which is in accordance with these requirements. It is based on components manufactured by Beckhoff Industrie Elektronik, Germany using the TwinCAT software package. A variety of different components are available off the shelf such as: servo controllers, stepping motor controllers, analogue to digital converts (ADCs), digital to analogue converters (DACs), digital I/O modules, etc. They are widely used in industrial applications such as numerical machining, automation, robotics, handling systems, etc. Vendor independent fieldbus systems such as SERCOS or EtherCAT can be used. There are very fast solutions for triggering and synchronisation of an arbitrary number of components in a system. So the requirements mentioned above can be fulfilled.

As a predecessor for an XFEL control system, the so-called Motion Control Test Undulator (MTU) has been setup at DESY to get hands-on experience using these components. An old decommissioned wiggler was refurbished using four motors and components now proposed for the XFEL. It was demonstrated, that the 'In Position' gap with enabled feedback can be controlled with an accuracy of 0.2 μm. Mechanical play and backlash, although detectable in the spindles, were fully compensated for by the encoder feedback. The synchronisation works reliably and the hardware allows for the synchronisation of external components as well. Because of this encouraging experience it now serves as a template for the control system for the XFEL prototype undulator segments.

5.4.4   Intersections

Between two adjacent undulator segments there is an intersection unit which contains a phase shifter, corrector coils and an adjustable quadrupole. Currently electromagnetic (EM) phase shifters using a three magnet chicane are foreseen **[5-62]**. In the same fashion, conventional EM quadrupoles mounted on horizontal/vertical remotely controlled movers are planned. The current time and cost planning foresees the use of EM technology for these devices. However, in the following two sections, alternative designs based on PM technology are discussed. This effort is driven by the goal of avoiding any source of heat in the undulator section in order not to jeopardise temperature stability, to make components in the intersection as short and compact as possible, to have a handle to control fringe fields and to have sufficient accuracy for adjustments of the quadrupole centre and its strength. There is yet another difference: EM quadrupoles are structures which completely enclose the electron beam. The insertion of a vacuum chamber after the calibration measurements is therefore problematic. In order to insert the vacuum chamber, three alternatives exist: Either the quadrupole has to be opened and closed; the chamber has to be welded in situ; or magnetic measurements must be made with the chamber already in place. Each of these procedures jeopardises precision on the μm

scale and/or complicates magnetic measurements and/or is difficult to perform in a clean room environment, which is required for the vacuum components of the XFEL. Planar permanent magnet quadrupoles (PPMQs) on the other hand are open to one side and may just be moved over the beam pipe. Here this problem does not exist.

5.4.4.1   Planar permanent magnet versus electro magnetic quadrupoles

An alternative to a conventional EM quadrupole is the PPMQ principle. It is an array of four magnetised parallelepipeds (see Figure 5.4.6). It is a modification of a proposal by Tatchyn [5-63]. A strong quadrupolar field is created in the centre of the PM array, which coincides with the beam axis. Two pairs of magnets, separated by a gap, are arranged as shown in Figure 5.4.6. The top and bottom separation distance may be changed independently by moving the blocks along the Z-direction symmetrically to the Y-axis. In this way, the gradient and the exact vertical centre position can be adjusted. These relations are shown in the contour plot in Figure 5.4.7 for European XFEL parameters. The gap is 12 mm. A maximum integrated gradient of about 8 T and a vertical centre adjustability of ±1 mm are required. Magnet dimensions are given in Figure 5.4.7 as well. It is seen that vertical centre adjustment capability requires some compromise with the integrated gradient, which has to be smaller than the maximum achievable one. 12 T is possible, at the cost of almost no adjustability. At 7.8 T the required adjustment range of ±1 mm is possible. Since the strength is proportional to the magnet length, a small increase might be needed to reach exactly 8 T. Horizontal centre adjustment is trivial: all four magnets may be moved by the desired amount along the Z-direction.
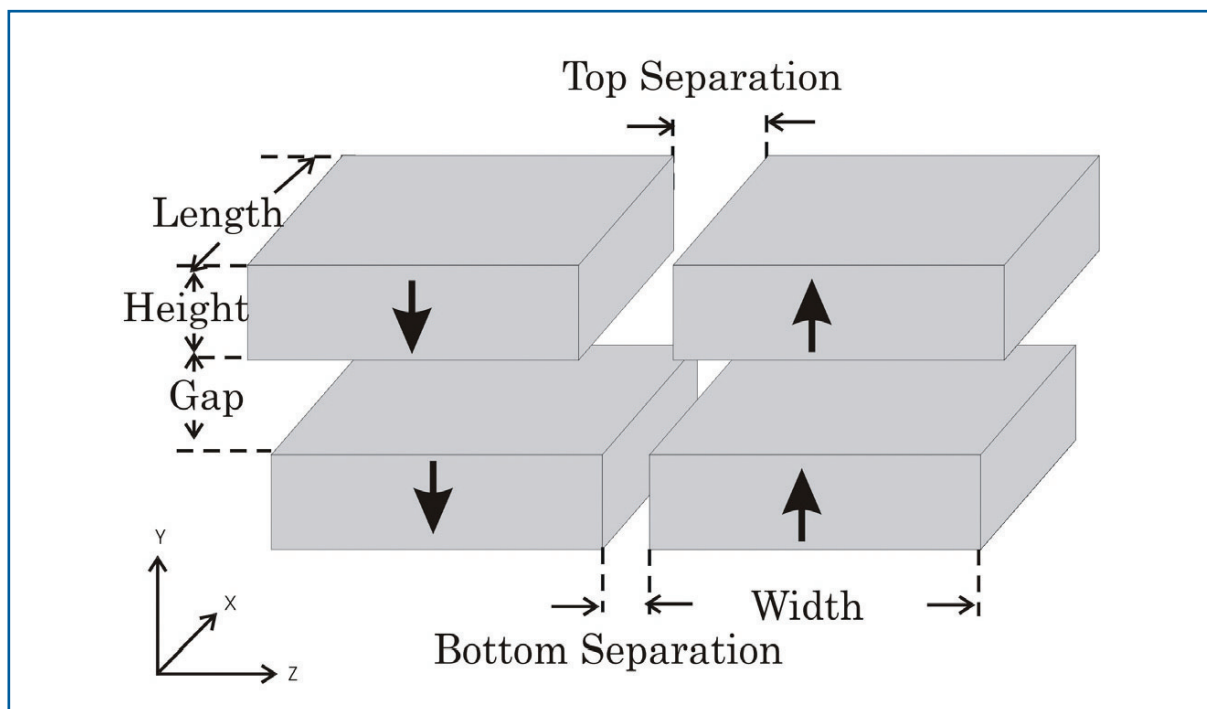

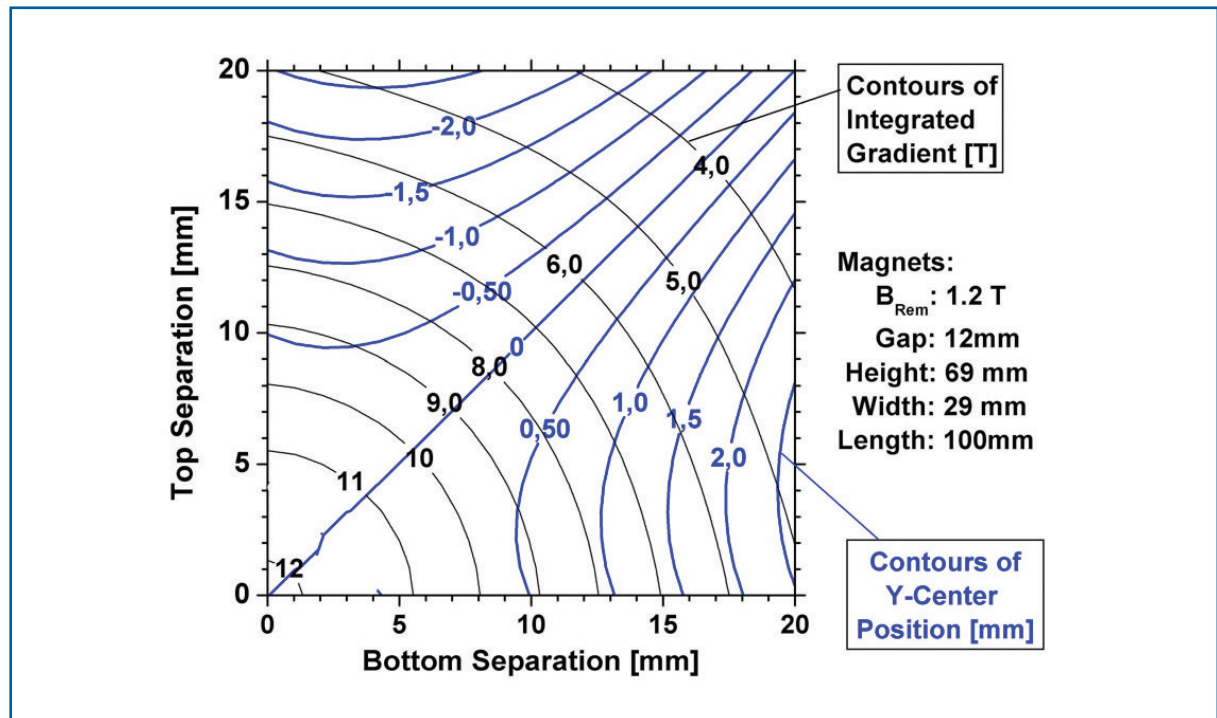**Figure 5.4.6**   *Principle of a PPMQ.*

Figure 5.4.7 *Contour plot of the field gradient and the position of the vertical centre as function of top and bottom separations.*

The good field area is about ±1.5 mm which is sufficient for an electron beam with an RMS beam size of typically 25 μm. Although it looks exotic, the PPMQ principle was heavily and successfully used in the undulator for the FEL at the TTF Phase 1 (TTF1) at 300 MeV. Magnet arrays similar to those in Figure 5.4.6 were superimposed to the field of a PM undulator [5-64]. A total of 30 planar PM quadrupoles were integrated in the 15 m long undulator section. Each quadrupole had an integrated strength of about 1.7 T. They were arranged to form a FODO lattice superimposed to the periodic field of the undulator. An average beta function in the whole 15 m long undulator section of 1 m has been achieved in this way. Adjustment and alignment of the quadrupoles were done in a similar fashion as discussed above [5-64, 5-65].

A PPMQ requires four precisely remotely controlled motorised axes. It may replace an EM quadrupole mounted on movable supports for beam steering as was described in [5-27]. This puts the additional mechanical effort for the PPMQ into perspective. The mechanical effort for a PPMQ is still larger than for an EM quadrupole on movable supports, but to compensate no power supply and cooling infrastructure is needed. So the cost difference is moderate. In the long-term, the operating cost of the PPMQ solution is, however, much lower anyway.

For the XFEL, control of the quadrupole centre positions with an accuracy of 1 μm is required. Whether the PPMQ principle meets this requirement depends not only on the stability, reproducibility and hysteresis of the permanent magnet material but also on the accuracy of the mechanical components used to move the magnets. This is subject to a detailed study. Assuming that these requirements can be fulfilled, each PPMQ can be

mapped out individually and with high precision in the same fashion as shown in Figure 5.4.7. In this way all errors can be individually characterised. Gradient and centre position can then be adjusted exactly by using these data.

It needs to be emphasised, that EM quadrupoles do not meet the above stability requirements a priori. Experience gained at FLASH has shown that differences in the coercive field of the Iron become visible at low excitation of the Iron and give rise to dipole components. As a consequence the magnetic centre moves by 50 μm and more depending on the current excitation and the magnetic history. The magnetic centre errors decrease with increasing current excitation. Special quadrupole designs using soft magnetic materials with very low coercive field, high permeability and sufficient saturation polarisation are needed. Such materials are used for special electro-mechanic applications such as actuators with low sticking effect, relays or low loss transformers. In a separate effort, EM quadrupoles using these materials are under development. A careful analysis and comparison of the PPMQ and the EM version will be performed before a final decision can be made.

5.4.4.2   *Electromagnetic versus permanent magnetic phase shifters*

In undulator systems with variable gaps, phase shifters are needed to exactly adjust the phase between segments so that constructive superposition of the emitted light occurs. The simplest one is a three magnet EM chicane. This solution was proposed in **[5-27]** and is described in detail in **[5-62]**. Drawbacks are hysteresis and asymmetries in the magnets, especially in the central one, space requirements and stray fields.

Figure 5.4.8 shows a sketch of a PM phase shifter, which avoids most of these drawbacks. It uses a zero potential yoke made of soft Iron, PMs and poles in a similar configuration as in the case of a hybrid undulator. The full centre magnets excite flux in the poles next to them with the same strength but opposite sign. So the field integral is always balanced. Additional magnets between poles and the zero potential yoke can be used to enhance the pole strength. Slight vertical movement of these magnets can be used for error correction. In addition the zero potential yoke very effectively terminates the field and avoids stray fields outside the phase shifter. Its strength is controlled via the gap. Parameters were calculated for an application in SASE 3 at minimum gap lasing at 1.6 nm, which is the worst case. Here, a total length (L) of 230 mm is needed. With a 30 mm thick Iron yoke and 9.5 mm long poles a peak field of 1.22 T at a gap of 10 mm can be obtained. With this shifter the phase can be delayed by $2.47 \times 2\pi = 15.5$ rad at 1.6 nm, which allows continuous phase adjustments over the whole wavelength range from 0.4 to 1.6 nm. During operation the phase shifter has to be moved with the gap in a synchronised fashion.
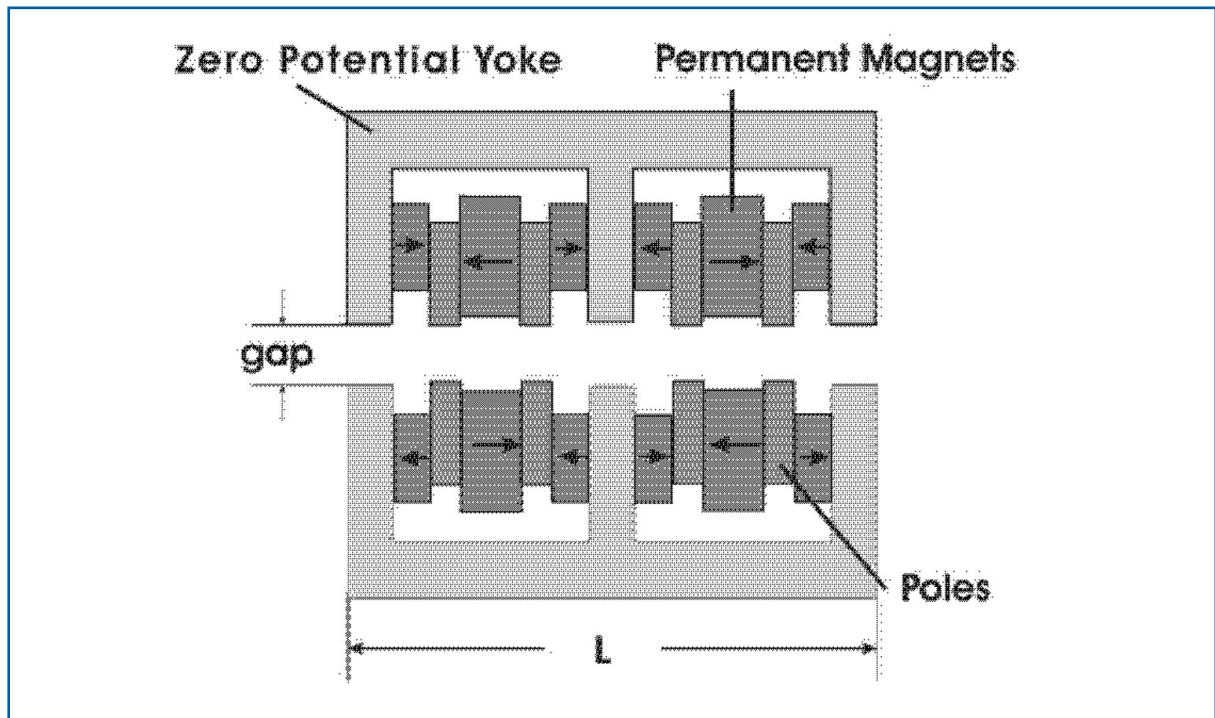
Figure 5.4.8   *Proposed PM phase shifter. The soft Iron zero potential yoke avoids stray fields. The strength can be adjusted by changing the gap. The length (L) is about 200 mm.*

5.4.5   Other components

For fine correction of residual field integral errors as a function of the gap, horizontal/vertical air coils are planned. They will be excited by a gap dependent current. Their maximum steering field integral is about 0.2 Tmm. Expected corrections, however, are much smaller, less than 0.05 Tmm. Air coils with similar properties, which are under development for the PETRA-III insertion devices, may be used for this purpose.

5.4.6   Implementation of undulator systems

The XFEL requires five undulator systems with the parameters shown in Table 5.4.1 to be operational by 2012/13. The scope of the whole construction effort is large and without precedent: the total magnetic length indicated in Table 5.4.1 is about three to four times that of a state-of-the-art third generation synchrotron radiation source such as APS, European Synchrotron Radiation Facility (ESRF) or Spring8.

Large scale production with heavy involvement of industrial partners will be an important part of the construction effort. Presently, there are very few vendors who have dedicated experience in building insertion devices mainly for use in storage rings. These are single items individually tailored to user requirements and are, therefore, quite expensive. But serial production, i.e. the production of a large number of identical or almost identical devices will be a mandatory aspect of the construction of the XFEL undulator systems. Vendors with suitable experience and capacity for large scale production of undulators do not yet exist. Vendor qualification is, therefore, essential to get qualified industrial partners involved.

Undulators for SASE and spontaneous emission

It is proposed to procure 'ready to use' undulator segments. Although some conditions and the total amount of work has changed compared to earlier estimates [5-27] this basic idea will be pursued and is the basis for further R&D activities, which can be subdivided into three steps:

Step 1 includes the definition and creation of a technological basis with involvement of industrial partners. This step is heavily affected by prior experience with the FLASH and includes:

• development of concepts for the mechanical design and motion control, which fully comply with XFEL requirements;

• construction of the first generation of prototypes, which in parallel are used for vendor qualification;

• development of fast and robust magnetic measurement techniques, which can be used in an industrial environment and are suited for large scale production;

• the first industrial study to elaborate on large scale production issues.

Some of these activities have already been started: a mechanical design and motion control concept, which has been described in this contribution, will be the basis for the first prototypes. They were built in 2006 as a first step to qualify vendors. In parallel, a new dedicated XFEL magnetic lab will be set up to develop magnetic measurement techniques. They are the prerequisites for the next step.

For step 2, there will be full involvement of industry including magnetic measurements and tuning. **Step 2** includes:

• incorporation of any design changes and imput from step 1;

• production of a second generation of prototypes, including the full production cycle;

• a second industrial study, which will be the basis for setting up large scale production.

Step 3 is the production phase and is planned to last for almost five years. It starts immediately after step 2 (but only if step 2 has been completed successfully). At this stage, the large scale production starts. Details will strongly depend on the experience gained during prototyping. However, the following points will be important:

• the placement of contracts;

• the planning of production capacities;

• the planning of production sites;

• work flow logistics;

• quality management, QA/QC procedures;

• a definition of the acceptance test;

• the start of serial production;

• the ramp up of production capacity.

A tentative time schedule, assuming that the undulator concept can be realised as described previously is shown in Table 5.4.3. The R&D phase, including two generations of prototypes (according to steps 1 and 2) has already started and will take in total four years. By 2010 everything is assumed to be ready for serial production. The SASE 1 system will be the first to become operational at the end of 2012, so has been started first. After its installation, commissioning of the XFEL will start. The SASE 2 system can be installed during the commissioning phase of SASE 1, and will become operational by the end of 2013. Therefore, it may be started with a delay of one year. The spontaneous systems U1 and U2 should be constructed and installed in parallel to SASE 2. For SASE 1, SASE 2, U1 and U2 the installation in the tunnels can be done parallel to the production since there is no beam in the tunnel. For SASE 3 this is different. This system will need much more construction effort. It is, therefore, postponed and will not become available before the end of 2014. Since SASE 1 is fully operational at this time, the installation will have to be done in a short shutdown of three months. There are no problems anticipated due to the short installation period of SASE 3. The time consuming installation of beamline components, such as vacuum chambers, intersections, etc. can be done previously in a shutdown. The SASE 3 undulator segments themselves will be installed quickly, since they are designed appropriately (see above). This will help to cut down installation time.

	2006	2007	2008	2009	2010	2011	2012	2013	2014
1. Prototype	■	■							
2. Prototype		■	■	■					
Serial Production									
SASE1									
Production					■	■	■		
Installation						■	■		
SASE2									
Production					▦	■	■	■	
Installation						■	■	■	
SASE3									
Production					▦	■	■	■	■
Installation									■
U1, U2									
Production					▦	■	■		
Installation						▦	■	■	

Table 5.4.3 *Tentative time schedule for undulator development and production for the XFEL. Start of operation is end of 2012.*

5.4.7 Summary

An update and overview over the undulator systems for the XFEL has been given. There are not only stringent tolerance requirements on the undulator systems for the XFEL, the construction of the large number of devices itself is also without precedent. A dedicated R&D programme, including the construction of prototypes, is being launched to provide the technological basis, to involve industry and qualify vendors. This R&D programme is the prerequisite for an effective serial production, which may start by 2010. The XFEL project is planned to start electron beam operation during years 2012/13. The last undulator system will be completed two years later. In this time frame the undulator systems have to be produced in the required numbers, in time, to budget and with sufficient quality.

5.5 Photon diagnostics of FEL radiation

FEL as well as spontaneous undulators of the XFEL, are multi-segmented systems with up to 42 single undulator cells. Alignment and commissioning of the numerous undulator cells along the XFEL beamline presents a serious challenge to measurement techniques based on electron beam (see Section 4.6 and **[5-66 – 5-68]**). Therefore, photon diagnostics provide an essential tool for commissioning and operation of the undulator cells independently of the electron-beam-based alignment procedure. Both methods will complement one another since the latter gives no insight into the magnetic gap or the phase match of adjacent undulator segments. Photon diagnostics have successfully been used at the TTF **[5-69]**, FLASH **[5-70, 5-71]**, the LEUTL FEL **[5-72]**, and has been proposed for the Linac Coherent Light Source (LCLS) project **[5-73, 5-74]**.

The concept of the photon-beam-based alignment procedure is based on variable gap undulator segments which allow the sampling of the spontaneous radiation of each segment individually by opening the gap of all other devices. With simultaneous measurement of photon beam position and angle, this radiation will be analysed with a special diagnostic station in order to:

- optimise angle and position of the electron beam trajectory;

- adjust the K-parameter of all undulator segments; and

- adjust the phase match between adjacent undulator segments.

In the following, the x-ray diagnostics for undulator system SASE 1 is discussed as a prototype representative for all beamlines. It is located about 460 m downstream of the last undulator cell (Figure 5.5.1) and allows characterising the radiation of an entire undulator system or individual segments and can be used for photon-beam-based alignment. It consists of a crystal monochromator as a principal unit, an imaging optics and different detector systems such as a CCD array, pin diodes, and a calorimeter. Since all undulators will be equipped with a gap drive, individual segments can be selected for diagnosis by switching off, i.e. opening the gap of all the other segments. This concept of only one common diagnostics for all undulator cells avoids a multiple installation of identical diagnostic devices which all would have to be calibrated against each other. In fact it facilitates a precise alignment and setup of the whole undulator system.

By observing only a limited area on the CCD it serves as a "virtual aperture", i.e. within the full area of the CCD array the angular acceptance can be set at time of data evaluation. However, an upper limit of 40 µrad (FWHM) is given by an aperture of 8 mm placed at the end of the last undulator (see Section 4.7.1.4). By a proper selection of the angular acceptance, one can get rid of Doppler-shifted higher harmonic and at the same time become less sensitive to electron divergence and beam direction jitter.
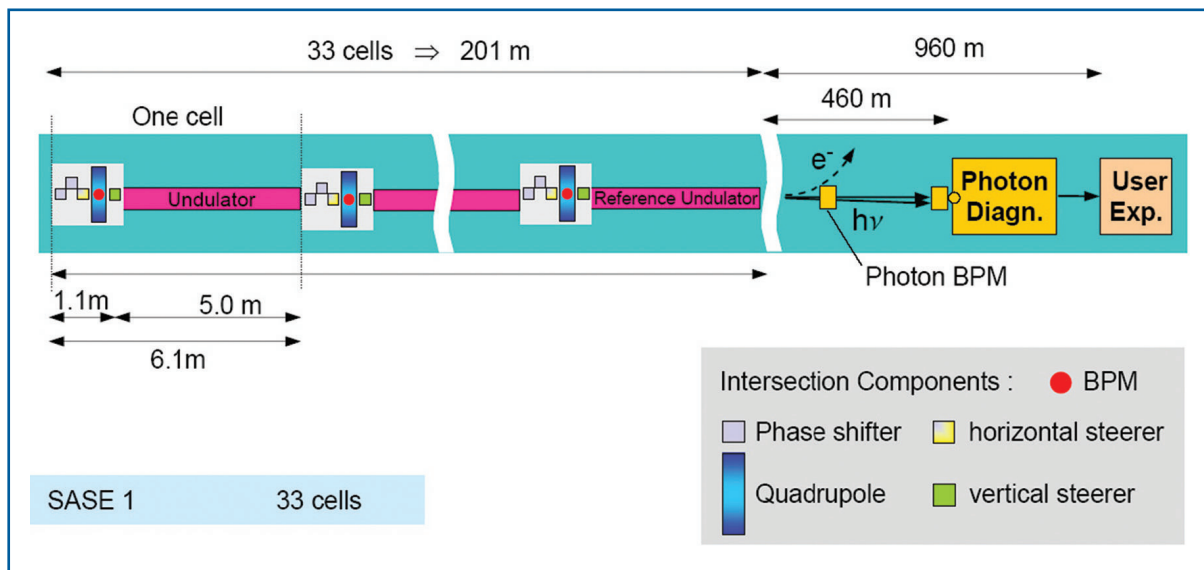
Figure 5.5.1   *Schematic layout of a XFEL beamline with photon diagnostics station.*

Fluctuations of electron beam parameters like electron charge and energy can be determined by a differential measurement technique. Following the concept proposed by B.X. Yang **[5-74]** the radiation from two undulator cells in parallel can be used: the last segment as a reference device (reference undulator) and one of the segments to be tested (test undulator). A steering magnet in the intersection upstream of the reference undulator deflects the electron beam horizontally by ~35μrad, so that the x-ray beam emitted from this undulator is well separated from the main axis, but allowed to pass the crystal monochromator of the diagnostic station. The x-ray beams from both segments are collected separately by the CCD array; hence, the radiation of the reference undulator can be used for normalisation.

Wave front calculations have been performed for the parameters of SASE 1 using SRW **[5-75]**, in order to estimate the properties of the undulator radiation of one or two segments observed at the diagnostic station. For ease of comparison, all calculations have been performed for an observation point 660 m downstream of the source. Table 5.5.1 summarises the corresponding photon beam parameters for the spontaneous radiation of one undulator segment. Three major diagnostic issues relate to a proper setup of the undulator cells, namely trajectory alignment, gap adjustment, and phase tuning. These are discussed in the following sections.

5.5.1   Trajectory alignment

It has been shown **[5-76]** that a random rms quadrupole offset of 1 μm will lead to a FEL gain reduction of ~10%. This value, corresponding to a second field integral of $I_2 = 83$ Tmm^2, is also considered as an upper limit of the trajectory displacement within a single undulator segment. The resulting requirement for angular trajectory alignment within a 5 m long undulator segment is 0.2 μrad. Spontaneous radiation of the first, third or fifth harmonic can be used for the different alignment aspects depending on the required accuracy. The top part of Figure 5.5.2 shows the energy spectrum of the first harmonics of

a single SASE 1 undulator segment for an electron beam with the nominal emittance. As expected, the emittance influence is still small for the (spontaneous) spectrum of the first harmonics. The lower part of Figure 5.5.2 displays spatial distributions for slightly different observation energies of the fundamental undulator peak. Detuning of the observation energy towards lower values leads to a broadening accompanied by a splitting of the intensity cone towards a ring. Detuning by 0.3% to higher energies (Figure 5.5.2c) leads to a considerable narrowing of the radiation cone, however, at the expense of lower intensity. The centre of gravity for all three intensity distributions in Figure 5.5.2 is on the beam axis independent of observing the radiation on- or off-crest of the undulator spectrum. Therefore, the photon beam axis and also the mean undulator trajectory, can be detected independently of a possibly incorrect gap setting. A still smaller spot size is obtained for higher harmonics of the undulator radiation.

Fundamental wavelength	0.1	nm
Fundamental photon energy	12.4	keV
Opening angle of fundamental σ	3.2	µrad
Footprint at 200 m (rms)	0.6	mm
Footprint at 600 m (rms)	2.1	mm

Table 5.5.1 *Photon beam parameters for the spontaneous radiation of one undulator segment. The electron beam energy is 17.5 GeV.*
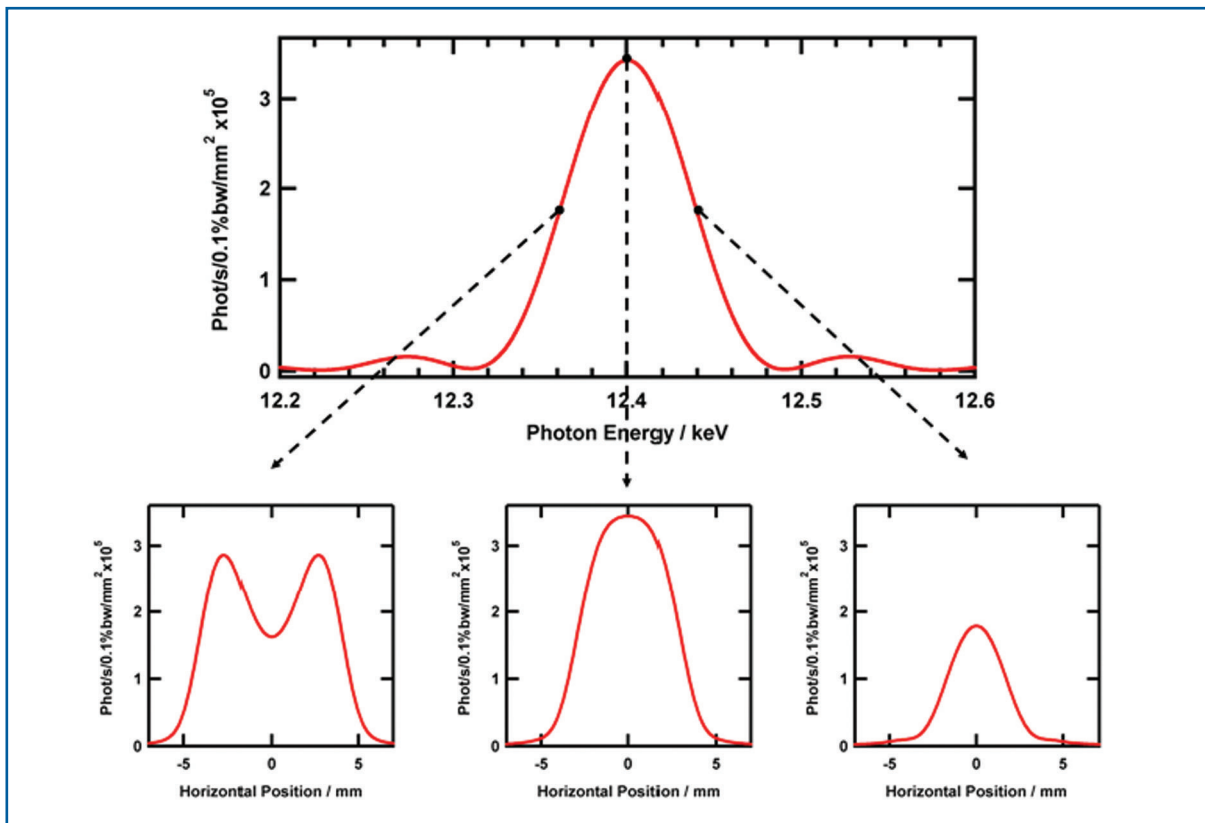

Figure 5.5.2 *Top part: Energy spectrum of the spontaneous radiation of a single 5 m long undulator segment of SASE 1 at a wavelength of ~0.1nm. Lower part (a–c): Profile of the circular beam expected for different observation energies (12.36, 12.40, 12.44 keV) in the vicinity of the undulator peak (arrows).*

Assuming a mean spatial line width of ~5.8 mm, an accuracy of ~2% of the FWHM (working with the first harmonic) or, correspondingly, 130 µm of the obtained spatial distribution, has to be achieved in order to cope with the specified angular resolution of 0.2 µrad. The setup described below will meet this requirement. The analysis of the photon spot as a single footprint of the electron trajectory through the undulator cannot distinguish between a shifted and a tilted orbit. Two photon BPMs will be installed between the undulator exit and the diagnostic station, which can be operated continuously without interference with a user experiment (Section 6.3).

5.5.2   Gap adjustment

One way to adjust the gap of each undulator segment is to take an energy spectrum whose centre of gravity defines the energy position of the undulator harmonics for the present gap value, which then has to be adjusted. The uncertainty in the measured fundamental energy has to be smaller than the ρ-parameter (4×10^{-4}), i.e. ~8 eV. Alternatively, the gap can be optimised by maximising the intensity at the desired photon energy which is then kept fixed. Corresponding to the ρ-parameter, the precision requirement for the gap adjustment is in the order of ~3 µm. Figure 5.5.3 displays the intensity obtained for fixed observation energy at the fundamental as a function of the gap detuning from its nominal value. It can be seen that the observed intensity varies considerably with a small gap misalignment. This method will work much faster than the first approach. Gap tuning of all undulator segments one by one will result in identical fundamental energies of all cells. A tiny taper of the gap along the entire undulator system, which is required to optimise the SASE intensity, has to be fine-tuned subsequently.
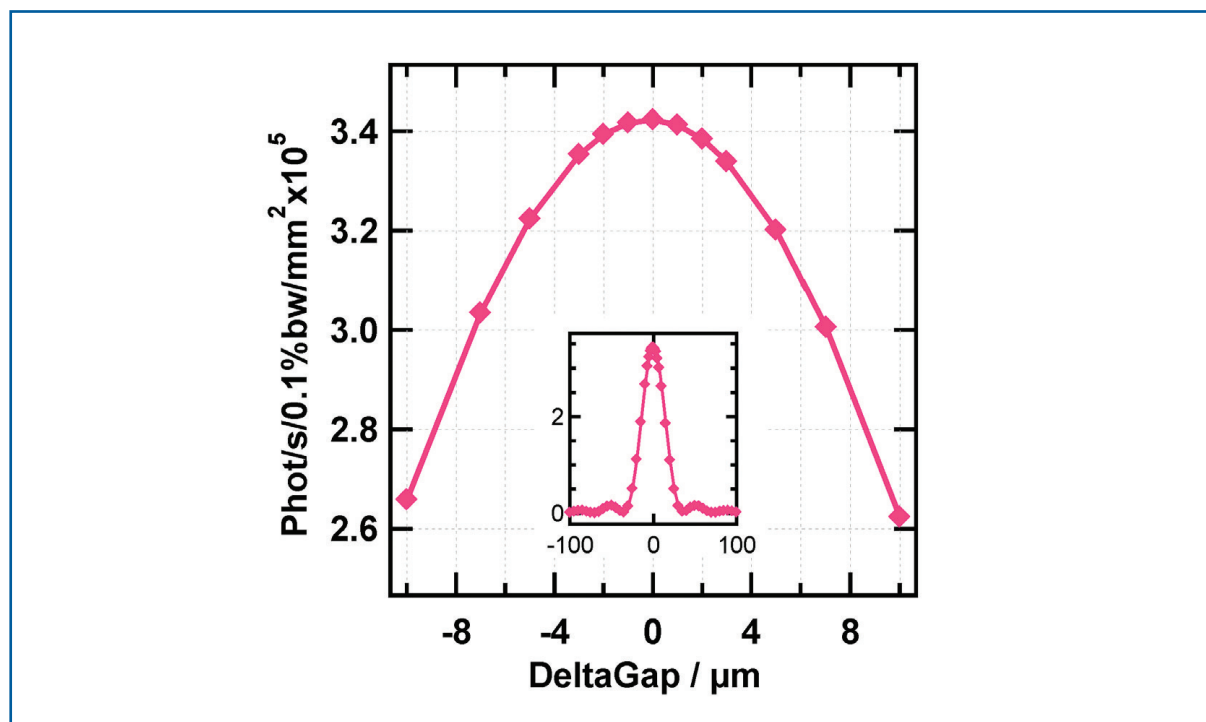

Figure 5.5.3   *Photon intensity as function of gap detuning for a constant observation energy of 12.4 keV (first harm.); the reference gap corresponds to the open gap position (10 mm).*

5.5.3   Phase tuning

Changing the undulator gap will result in a change of the phase relation between two adjacent segments. In order to compensate for the wavelength dependent phasing condition, a phase shifter is installed in the intersection module (Section 5.4.4). It consists of a three-magnet chicane which is powered by a gap-dependent current, and delays the electron beam so that the radiation from the following segment is in phase with that of the previous for all wavelengths. The adjustment of the optical phase has to be assured with an accuracy of only ~1%, i.e. a few degrees [5-77]. The determination of the correct phase is based on observing the radiation of two successive undulator segments. The phase relation affects the energy spectrum as well as the spatial distribution of the composed radiation. For complete phase match, the undulator line peaks at E_{fund}: In case of fully destructive interference, the undulator spectrum shows intensity maxima below and above that value. The spatial radiation distribution at $E = E_{fund}$ is cone-like in the matched phase condition, whereas the radiation is emitted in a ring in the destructively interfering case. The easiest way to monitor the phase is to observe the photon intensity at constant energy $E_{obs} = E_{fund}$ while shifting the optical phase in the electron chicane. The detected photon flux shows cosine dependence with a peak-to-peak amplitude ratio of ~700 for a phase advance from π to 2π (Figure 5.5.4). This will be sufficient to tune the optical phase within the required accuracy.
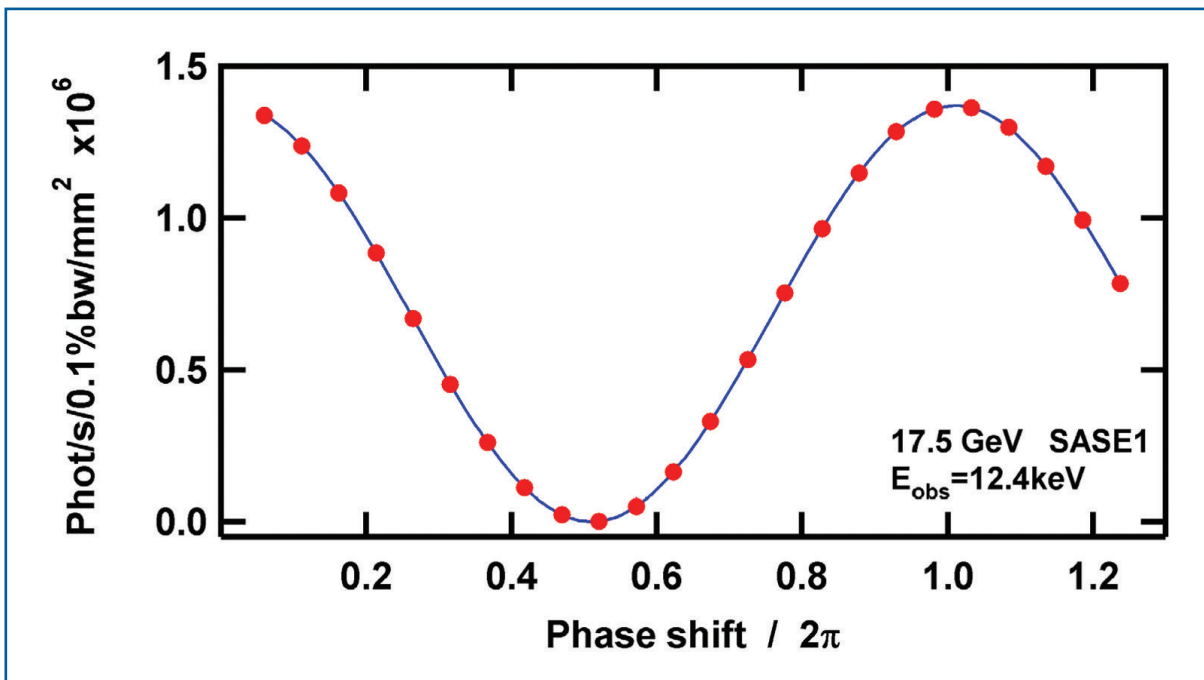

Figure 5.5.4   *Simulation of the phase dependent intensity variation using the SRW code. While changing the operating conditions from an anti- to a phased mode one observes a difference in intensity by a factor of 700.*

5.5.4 Hardware setup

The photon diagnostic station consists of three parts: the photon beam position monitors, the central imaging station, and a detector unit for observation of integral properties. Photon BPMs will be used in conjunction with the imaging station to precisely align the trajectories of all undulator segments, in particular to distinguish between transversal and angular displacement. Position-sensitive ionisation chambers are present state-of-the-art photon monitors in terms of resolution and are most appropriate for this application as they do not directly interact with the beam (see Section 6.2). The primary part of the photon diagnostic station will image the central cone of the monochromatic beam of the test and reference undulator in parallel. It will be possible to observe an image at the energy of the first and fifth harmonic of the XFEL undulator through two different view ports. A field of view with a diameter of 50 mm is needed in order to disentangle the radiation cones of both the reference and the test undulator and to determine their FWHM and shape. The undulator beam will be monchromatised using a single crystal Laue-case setup similar to that used at the PETRA-undulator beamline at DESY as shown in Figure 5.5.5. There will be two fixed view ports in order to observe the first and fifth harmonic of the undulator by only rotating the crystal. The observation of two angles allows the determination of an absolute energy scale.
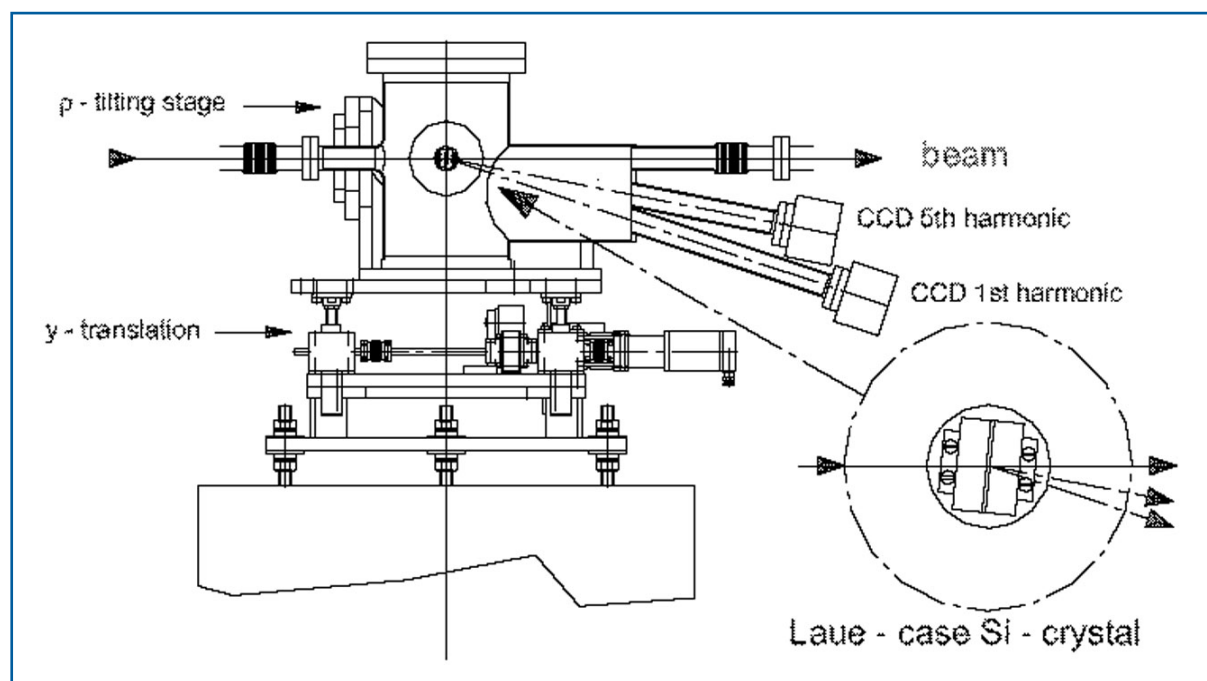

Figure 5.5.5 *Schematic view of the diagnostic station setup. A Laue-case Silicon crystal monchromatises the undulator radiation. The central cone will be observed at two photon energies (first and fifth harmonics) through fibre optic view ports coated with fluorescent screens.*

Experience with a similar setup at the PETRA beamline (Section 5.5.5) with the PETRA storage ring at DESY running at 12 GeV positron energy, shows that the images obtained by a thin Laue-case crystal with a thickness of 200 µm provide a clear picture without additional spots and high energy background. The Laue-case setup is favourable due to

the small Bragg angles of 5.49° and 9.17° required for the fifth harmonic using Si (3 3 3) and for the first harmonic with Si (1 1 1), respectively.

An imaging system is proposed using a Laue-case crystal to monochromatise the central cone of the test and reference undulator, projecting them onto a fluorescent screen attached directly onto a fibre optic taper. The fluorescent screen will be either directly coated onto the fibre or be a thin film screen attached to it. This taper is part of a fibre optic vacuum window. At the airside of this window, a CCD chip will be directly bonded onto the fibre. Assuming a field of view of 50 mm^2 and the need for a 12 µm^2 pixel size (16-bit resolution requirement), a taper with an imaging ratio of 2:1 (screens side: CCD side) will be installed. The overall resolution of the system using a 2,048 $\times$ 2,048 pixel CCD will be 24 µm^2 /pixel. An option will be replacing the fluorescent screen coating at the fibre end by a doping of the fibre end.

Present day 16-bit resolution CCD systems are driven with a maximum pixel clock of 50 kHz, due to an increase in readout noise at higher clock rates. The dark current in a cooled CCD system is negligible at exposure times in the seconds range. Under these conditions, the setup will be able to provide an image every 20 s. A 12-bit system would provide an image in 1 s or faster, but the dynamic range is too limited to observe the effect of phasing two undulator segments without changing the exposure time. Integral beam properties of both the spontaneous and SASE radiation will be determined in a second station.

5.5.5 Test at PETRA II

First tests of the basic diagnostic scheme have been successfully performed at the PETRA-II storage ring operating at 12 GeV **[5-78, 5-79]**. Here, a similar setup using BPMs for stabilisation and a cryogenically cooled Silicon crystal in Laue geometry in combination with a fluorescent screen and CCD imager, have been used for emittance measurements. Figure 5.5.6 shows a set of images of the first harmonic of the undulator for a variation of the undulator gap from 18 to 21 mm, corresponding to 21.23 keV at 18.8 mm. Gaussian fits to horizontal lines through the centre of mass in all images provide the standard deviation of the measured intensity distributions in the horizontal plane. The images are processed in order to obtain the standard deviation of the width of the photon beam. The results are depicted in Figure 5.5.7. For each image, the integrated intensity, the shape of the horizontal beam profile through the centre of mass (kurtosis), and the variance values, are determined and plotted against the gap setting. Figure 5.5.7 shows that only at the gap setting yielding the maximum intensity, does the profile have a true Gaussian shape and coincide with the smallest variance, corresponding to the smallest FWHM of the profile.
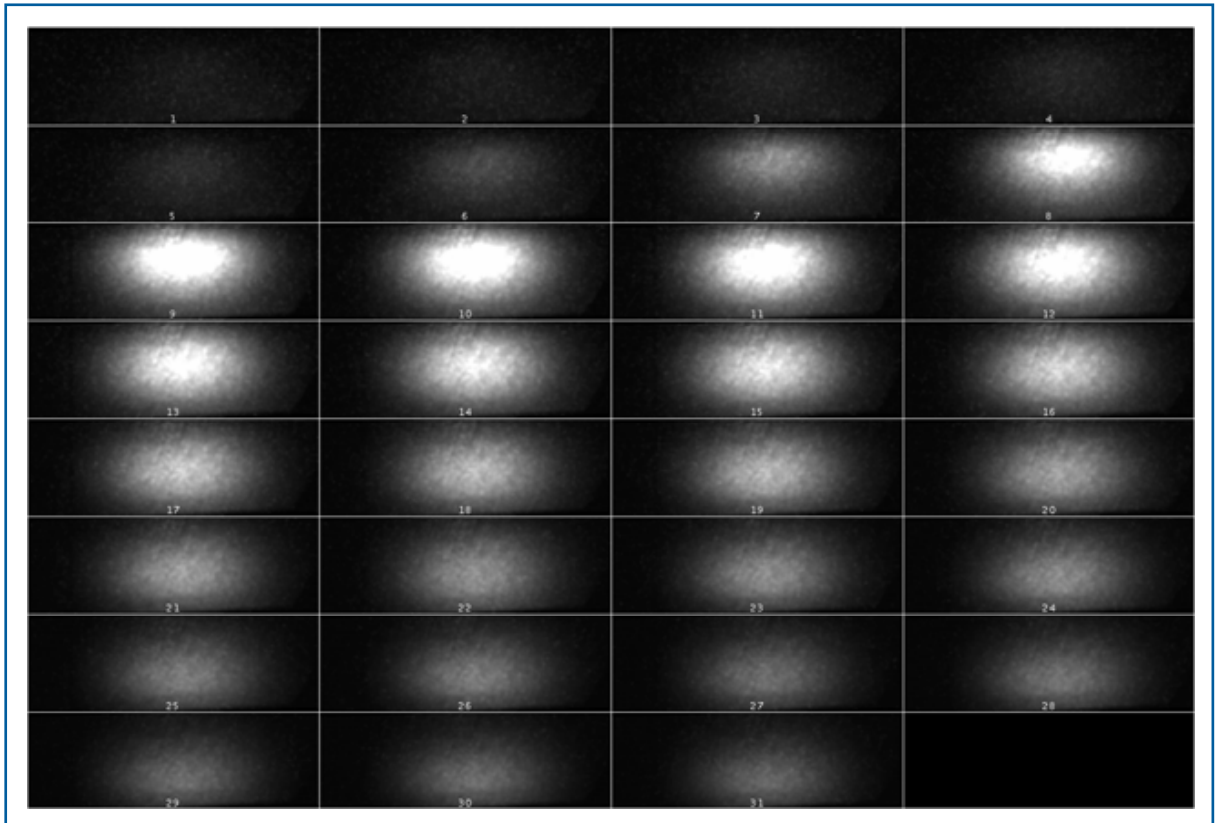
Figure 5.5.6   *Set of images taken with a fixed exposure time showing the mono-chromatised photon beam at a fixed crystal setting corresponding to a photon energy of the first undulator harmonic of 21.23 keV. The setting of the undulator gap ranges from 18 mm to 21 mm magnetic gap in steps of 0.1 mm (top left image #1 at 18 mm, bottom right image #31 at 21 mm).*
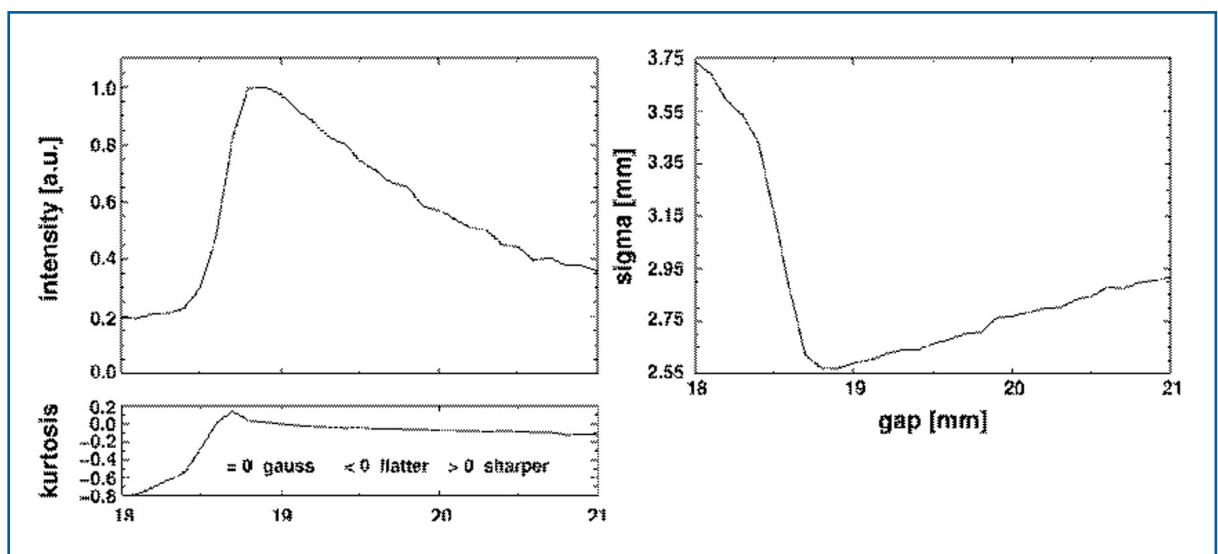

Figure 5.5.7   *Left: integrated intensity in each image and the Gauss-likeliness of the line shape of a horizontal cut through the centre of mass in each image. Right: calculated variance of all line scans.*

5.6 Future extensions to the European XFEL Facility

The present Technical Design Report describes the basic option of the European XFEL Facility. However, during our design work we foresee physical and technical solutions which will allow significant performance enhancements without significant changes to the infrastructure and hardware. These potential extensions are high-power (sub-TW level) mode of operation, two-colour mode of operation (frequency doubler), and attosecond mode of operation **[5-80]**. The present concept of undulator can be easily modified for operation in high- power and two-colour modes of operation (as illustrated in Figure 5.6.1). Both schemes are realised in a simple way by replacement of one of the undulator modules by a dispersion section, and essentially use the feature of a small energy spread in the electron beam allowing effective enhancement of the beam bunching. Application of the undulator tapering in the final part of the undulator allows production of ultra-high power radiation pulses. Figure 5.6.2 shows the temporal structure of the radiation pulse for SASE 2 undulator tuned to high power mode of operation.

In its simplest configuration, the frequency doubler consists of an input undulator, and an output undulator separated by a dispersion section (see Figure 5.6.1) **[5-81]**. After passing through the dispersion section, the bunched beam has not only a fundamental radiation frequency component, but also considerable intensity in its harmonics. It is possible to have an input undulator operating at one frequency, and an output undulator operating at double this frequency. The radiation in the output undulator will then be excited by the harmonic component in the electron beam, and the FEL will operate as a combination of frequency multiplier and amplifier.
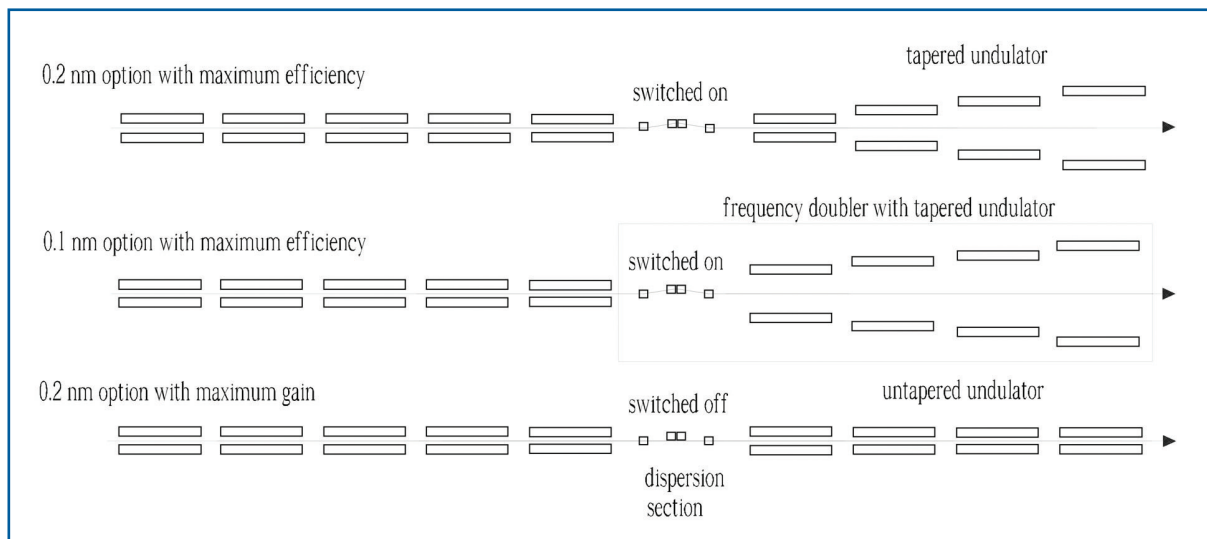

Figure 5.6.1   *Three different modes of operation of SASE undulator. Top: high power option; middle: frequency doubler; bottom: standard SASE. Only one type of undulator magnet structure is used. The radiation wavelength will be tuned by changing the gap* **[5-80].**
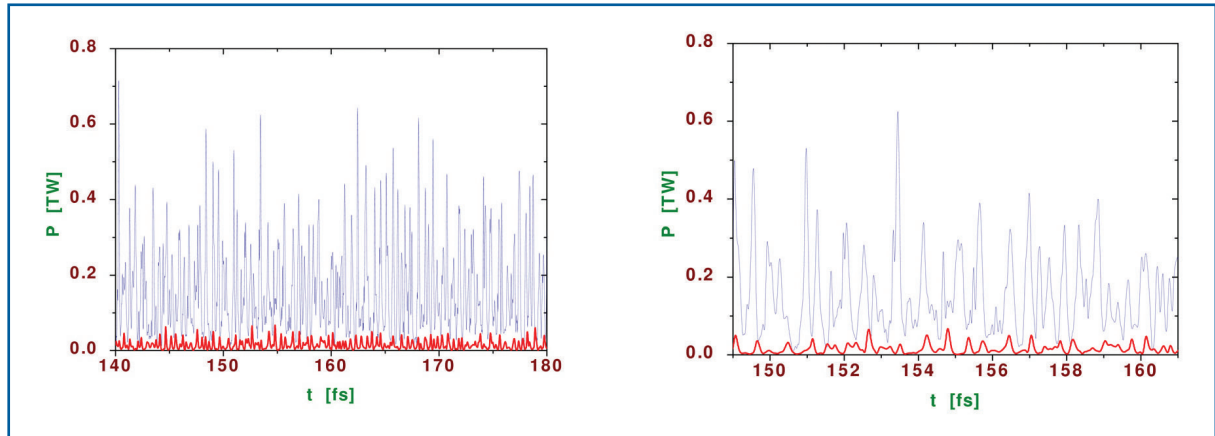
Figure 5.6.2 *Temporal structure of the radiation pulse for SASE 2 at 0.2 nm tuned for high power mode of operation. Right plot shows enlarged view of the left plot. The red line shows radiation pulse for the basic option (see Figure 5.2.4). The undulator length is 150 m.*

A technique for the production of attosecond x-ray pulses is based on the use of x-ray SASE FEL combined with a femtosecond laser system **[5-82, 5-83]** (see Figure 5.6.3). An ultrashort laser pulse is used to modulate the energy of electrons within the femtosecond slice of the electron bunch at the seed laser frequency. The seed laser pulse will be timed to overlap with the central area of the electron bunch. It serves as a seed for a modulator which consists of a short (a few periods) undulator. Following the energy modulator the beam enters the x-ray undulator. The process of amplification of radiation in this undulator develops in the same way as in a conventional x-ray SASE FEL: fluctuations of the electron beam current serve as the input signal. The proposed scheme for the generation of attosecond pulses is based on frequency-chirping the SASE radiation pulse. When an electron beam traverses an undulator, it emits radiation at the resonance wavelength $\lambda=\lambda_u(1+K_{rms}^2)/(2\gamma^2)$. The laser-driven sinusoidal energy chirp produces a correlated frequency chirp of the resonant radiation $\delta\omega/\omega=2\delta\gamma/\gamma$. After the undulator, the radiation is passed through a crystal monochromator which selects a narrow bandwidth. Since the radiation frequency is correlated to the longitudinal position within the beam, a short temporal radiation pulse is transmitted through the monochromator. A modification of the attosecond XFEL concept uses undulator detuning for selection and amplification of ultra-high power attosecond pulses (see Figure5.6.4 **[5-83]**).

The attosecond x-ray pulse is naturally synchronised with its femosecond optical pulse which opens a unique perspective for pump-probe experiments with sub-femtosecond resolution. It is important that the attosecond scheme is based on the nominal XFEL parameters, and operates in a "parasitic" mode, not interfering with the main mode of the XFEL operation. It can be realised with minimum additional efforts. The machine design should foresee the space for the installation of a modulator undulator and a view port for the input optical system. Many of the components of the required laser system can be achieved with technology which is currently being developed for applications other than the attosecond x-ray source.
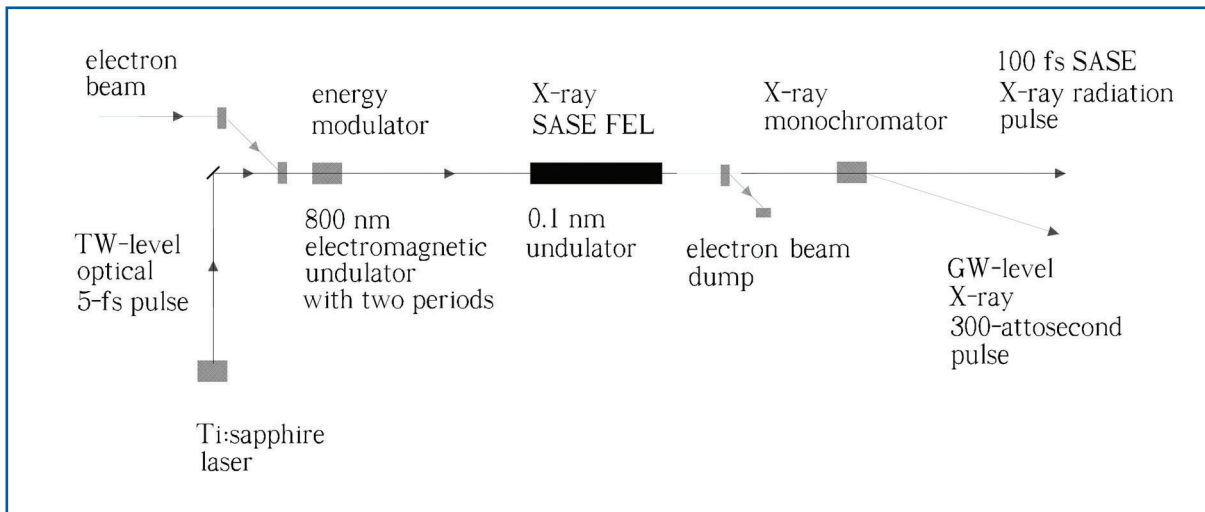
Figure 5.6.3 *Schematic diagram of attosecond x-ray source* **[5-82]**.
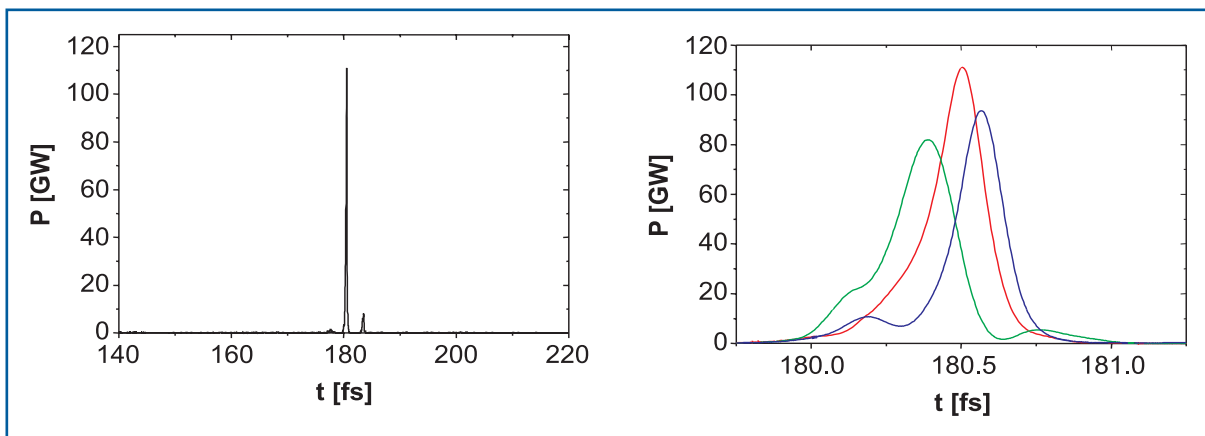

Figure 5.6.4 *Temporal structure of the radiation pulse from an ultra-high power attosecond XFEL* **[5-83]**. *Right plot shows enlarged fraction of a central peak. The lines correspond to three different shots.*

A single pass x-ray SASE FEL can be modified as proposed in **[5-84, 5-85]** to significantly reduce the bandwidth and the fluctuations of the output radiation. The modified scheme consists of two undulators with an x-ray monochromator located between them. The first undulator operates in the linear regime of amplification starting from the shot noise, and the output radiation has the usual SASE properties. After the first undulator, the electron beam is guided through a bypass and the x-ray beam enters the monochromator which selects a narrow band of radiation. At the entrance of the second undulator, the monochromatic x-ray beam is combined with the electron beam and is amplified up to the saturation level. The scheme is shown in Figure 5.6.5.
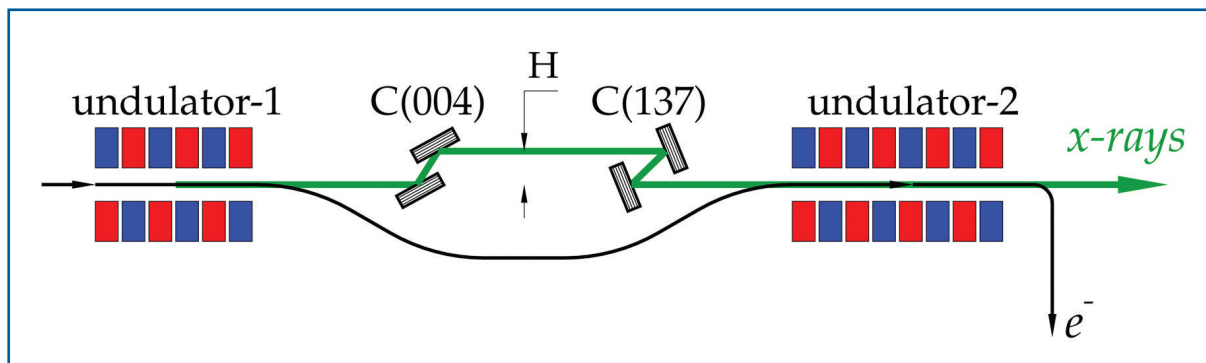
Figure 5.6.5 *Schematic layout of the two-stage FEL with the SASE FEL (left), a mono-chromator and electron debuncher (middle) and an amplifier (right)* **[5-85]***.*

Possible extensions of the European XFEL should foresee both extension of the quality of the photon beam properties, and extension of the number of user stations which can operate simultaneously (or, quasi-simultaneously). An x-ray photon beam from a SASE FEL undulator is in principle a single user tool, just like an optical laser. Therefore, the operation and amortisation cost cannot be easily spread over many simultaneous experiments. To avoid prohibitive cost for each experiment, a perspective extension of XFEL laboratory has been proposed **[5-80]**. In this scenario all electrons will be guided into only one electron beamline including three undulator systems and the dump (Figure 5.6.6).
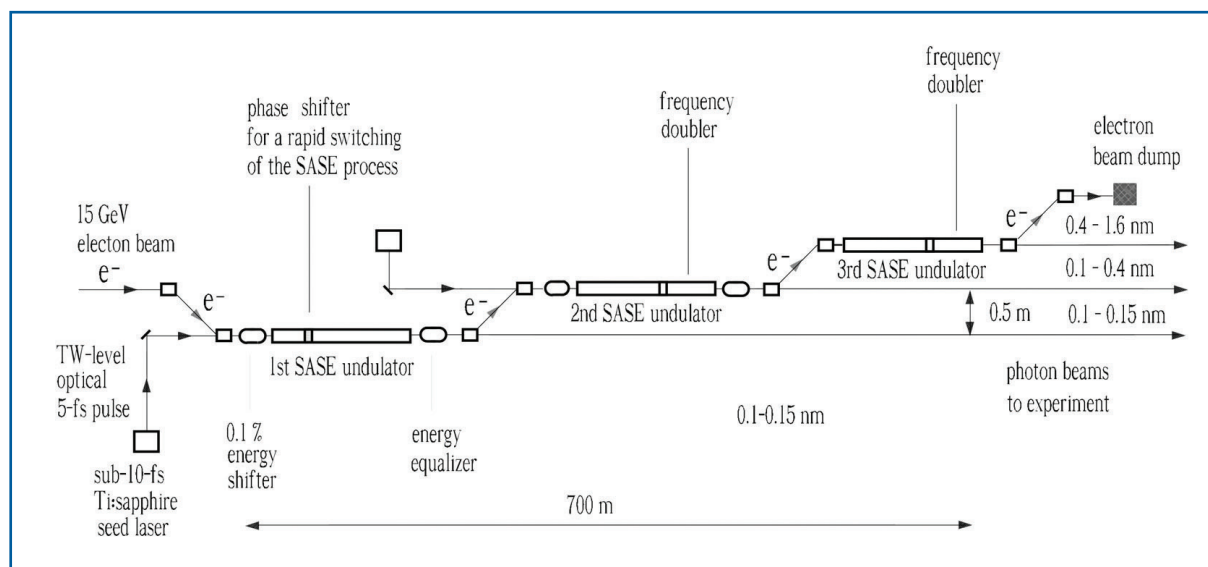

Figure 5.6.6 *Sketch of an x-ray SASE FEL source providing multi-user capability* **[5-80]**.

Using a 0.1% electron (photon) energy shifter in a SASE undulator, it is possible to rapidly turn off the FEL gain, thereby enabling users to switch effectively from one XFEL to another. This technique could provide quasi-simultaneous operation of all three XFELs in one electron beamline. Using a photon beam distribution system based on movable optics could thus enable many independent beamlines to work in parallel, thereby providing much more time for user experiments. The present layout of the European XFEL would

accommodate such an extension, and an appropriate increase of the tunnel diameter has been included in the project.

5.7 Summary of costs and manpower requirements

The capital investment and cost of the personnel necessary to build the undulator system as described in the previous sections of this chapter are summarised in this section. The basis for the cost estimate is the system layout and the parameters specified here. For an overview about the total project cost, a description of the methodology of the performed estimate for capital investment, the determination of the costs for personnel and the expected uncertainties, see Chapter 10.

Table 5.7.1 gives a summary of the project cost in terms of capital investment and the cost of personnel for the undulator systems. The undulator systems contribute about 10% to the overall project cost. Integrated over the entire construction phase, 149 Full-Time Equivalents (FTE) are required for the undulator system.

	Capital Investment [M€]	Personnel Cost [M€]	Full Cost [M€]
Undulator Systems	56.52	12.10	68.62

Table 5.7.1 *Capital investment, personnel costs and full costs in Million-Euro for the undulator system.*

Undulator system: design, construction, magnetic measurement, installation and commissioning of the undulators systems SASE 1 to 3 and U1 and U2 with mechanical support, magnetic structures, motion control, and FEL simulation software. Undulator systems are composed of a certain number of undulator segments and the required instrumentation for electron beam fine correction placed in the intersections between segments. The number of segments is determined by the longest saturation length for the design range of photon energies. Undulators for spontaneous radiation have been designed to be ten segments long.

References

[5-1]   R.H. Pantell, Y. Soncini, and H.E. Putthoff, *Stimulated Photon-Electron Scattering*, IEEE J. Quant. Electr. 11 (1968) 905.

[5-2]   J.M.J. Madey, *Stimulated Emission of Bremsstrahlung in a Periodic Magnetic Field*, J. Appl. Phys. 43 (1972) 3014.

[5-3]   A.M. Kondratenko and E.L. Saldin, *Generation of Coherent Radiation by a Relativistic Electron Beam in an Undulator*, Part. Accelerators 10 (1980) 207.

[5-4]   Ya.S. Derbenev, A.M. Kondratenko and E.L. Saldin, *On the Possibility of Using a Free-Electron Laser for Polarisation of Electrons in Storage Rings*, Nucl. Instrum. and Methods 193 (1982) 415.

[5-5]   R. Bonifacio, C. Pellegrini and L.M. Narducci, *Collective Instabilities and High-Gain Regime in a Free-Electron Laser*, Opt. Commun. 50 (1984) 373.

[5-6]   J.B. Murphy and C. Pellegrini, *Free electron lasers for the XUV spectral region*, Nucl. Instrum. and Methods A 237 (1985) 159.

[5-7]   E.L. Saldin, E.A. Schneidmiller, M.V. Yurkov, *The Physics of Free Electron Lasers*, Springer-Verlag, Berlin (1999).

[5-8]   K.J. Kim, *Three-Dimensional Analysis of Coherent Amplification and Self-Amplified Spontaneous Emission in Free-Electron Lasers*, Phys. Rev. Lett. 57 (1986) 1871.

[5-9]   J.M. Wang and L.H. Yu, *A transient analysis of a bunched beam free electron laser*, Nucl. Instrum. and Methods A 250 (1986) 484.

[5-10]   S. Krinsky and L.H. Yu, *Output power in guided modes for amplified spontaneous emission in a single-pass free-electron laser*, Phys. Rev. A 35 (1987) 3406.

[5-11]   M. Xie, *Exact and variational solutions of 3D eigenmodes in high gain FELs*, Nucl. Instrum. and Methods A 445 (2000) 59.

[5-12]   E.L. Saldin, E.A. Schneidmiller and M.V. Yurkov, *The general solution of the eigenvalue problem for a high-gain FEL*, Nucl. Instrum. and Methods A 475 (2001) 86.

[5-13]   E.L. Saldin, E.A. Schneidmiller and M.V. Yurkov, *Statistical properties of radiation from VUV and X-ray free electron laser*, Opt. Commun. 148 (1998) 383.

[5-14]   E.L. Saldin, E.A. Schneidmiller and M.V. Yurkov, *Diffraction effects in the self-amplified spontaneous emission FEL*, Opt. Commun. 186 (2000) 185.

[5-15] E.L. Saldin, E.A. Schneidmiller and M.V. Yurkov, *Nonlinear simulations of FEL amplifier with an axisymmetric electron beam*, Opt. Commun. 95 (1993) 14.

[5-16] E.L. Saldin, E.A. Schneidmiller, and M.V. Yurkov, *Simulation studies of a 6 nm Free Electron Laser at the TESLA test facility starting from noise*, Nucl. Instrum. and Methods A 393 (1997) 157.

[5-17] P. Pierini and W. Fawley, *Shot noise startup of the 6 nm SASE FEL at the TESLA test facility*, Nucl. Instrum. and Methods A 375 (1996) 332.

[5-18] E.L. Saldin, E.A. Schneidmiller, and M.V. Yurkov, *FAST: a three-dimensional time-dependent FEL simulation code*, Nucl. Instrum. and Methods A 429 (1999) 233.

[5-19] S. Reiche, *GENESIS 1.3: a fully 3D time-dependent FEL simulation code*, Nucl. Instrum. and Methods A 429 (1999) 243.

[5-20] V. Ayvazyan et al., *Generation of GW Radiation Pulses from a VUV Free-Electron Laser Operating in the Femtosecond Regime*, Phys. Rev. Lett. 88 (2002) 104802.

[5-21] V. Ayvazyan et al., *A new powerful source for coherent VUV radiation: Demonstration of exponential growth and saturation at the TTF free-electron laser*, Eur. Phys. J. D 20 (2002) 149.

[5-22] M. Dohlus et al., *Start-to-end simulations of SASE FEL at the TESLA Test Facility, phase 1*, Nucl. Instrum. and Methods A 530 (2004) 217.

[5-23] E.L. Saldin, E.A. Schneidmiller, M.V. Yurkov, *Expected Properties of the Radiation from VUV-FEL at DESY (Femtosecond Mode of Operation)*, TESLA-FEL report 2004-06, DESY, Hamburg (2004).

[5-24] E.L. Saldin, E.A. Schneidmiller, M.V. Yurkov, *Statistical Properties of the Radiation from VUV FEL at DESY Operating at 30 nm Wavelength in the Femtosecond Regime*, DESY report 2005-239, DESY, Hamburg (2005).

[5-25] V. Ayvazyan et al., *First operation of a free-electron laser generating GW power radiation at 32 nm wavelength*, Eur. Phys. J. D 37 (2006) 297.

[5-26] *Conceptual Design of 500 GeV e+e- Linear Collider with Integrated X-ray Facility*, R. Brinkmann et al.(Eds.), DESY report 97-048, DESY, Hamburg (1997).

[5-27] *TESLA Technical Design Report Part V, The X-ray Free Electron Laser*, G. Materlik, T. Tschentscher (Eds.), DESY report 2001-011, DESY, Hamburg (2001), http://tesla.desy.de/new_pages/0000_TESLA_Project.html

Undulators for SASE and spontaneous emission – References

[5-28] *TESLA XFEL Technical Design Report Supplement*, R. Brinkmann, B. Faatz, K. Flöttmann, J. Rossbach, J. Schneider, H. Schulte-Schrepping D. Trines, T. Tschentscher, H. Weise (Eds.), DESY report 2002-167, DESY, Hamburg (2002), http://tesla.desy.de/new_pages/0000_TESLA_Project.html

[5-29] E.L. Saldin, E.A. Schneidmiller and M.V. Yurkov, *The Potential for Extending the Spectral Range Accessible to the European X-ray Free Electron Laser in the Direction of Longer Wavelengths*, TESLA FEL report 2004-05, DESY, Hamburg (2004).

[5-30] E.L. Saldin, E. A. Schneidmiller, and M.V. Yurkov, *Design formulas for short-wavelength FELs*, Opt. Commun. 235 (2004) 415.

[5-31] J. Rossbach, E.L. Saldin, E.A. Schneidmiller and M.V. Yurkov, *Interdependence of parameters of an X-ray FEL*, Nucl. Instrum. and Methods A 374 (1996) 401.

[5-32] E.L. Saldin, E.A. Schneidmiller, and M.V. Yurkov, *Calculation of energy diffusion in an electron beam due to quantum fluctuations of undulator radiation*, Nucl. Instrum. and Methods A 381 (1996) 545.

[5-33] E.L. Saldin, E.A. Schneidmiller and M.V. Yurkov, *Coherence properties of the radiation from SASE FEL*, Nucl. Instrum. and Methods A 507 (2003) 106.

[5-34] E.L. Saldin, E.A. Schneidmiller and M.V. Yurkov, *Coherence properties of the radiation from X-ray free-electron laser*. Proceedings of the FEL 2006 Conference, Berlin.

[5-35] M. Schmitt and C. Elliot, *Even-harmonic generation in free-electron lasers*, Phys. Rev. A 34 (1986) 6.

[5-36] R. Bonifacio, L. De Salvo, and P. Pierini, *Large harmonic bunching in a high-gain free-electron laser*, Nucl. Instrum. and Methods A 293 (1990) 627.

[5-37] W.M. Fawley et al., *Large harmonic bunching in a high-gain free-electron laser*, Proc. IEEE Part. Acc. Conf., (1995) 219.

[5-38] H. Freund, S. Biedron and S. Milton, *Nonlinear harmonic generation and proposed experimental verification in SASE FELs*, Nucl. Instrum. and Methods A 445 (2000) 53.

[5-39] H. Freund, S. Biedron and S. Milton, *Nonlinear Harmonic Generation in Free-electron Lasers*, IEEE J. Quant. Electr. 36 (2000) 275.

[5-40] S. Biedron et al., *Measurements of nonlinear harmonic generation at the Advanced Photon Source's SASE FEL*, Nucl. Instrum. and Methods A 483 (2002) 94.

[5-41] S. Biedron et al., *Impact of electron beam quality on nonlinear harmonic generation in high-gain free-electron lasers*, Phys. Rev. ST 5 (2002) 030701.

Undulators for SASE and spontaneous emission – References

[5-42] Z. Huang and K. Kim, *Three-dimensional analysis of harmonic generation in high-gain free-electron lasers*, Phys. Rev. E 62 (2000) 7295.

[5-43] Z. Huang and K. Kim, *Nonlinear harmonic generation of coherent amplification and self-amplified spontaneous emission*, Nucl. Instrum. and Methods A 475 (2001) 112.

[5-44] A. Tremaine et al., *Experimental Characterization of Nonlinear Harmonic Radiation from a Visible Self-Amplified Spontaneous Emission Free-Electron Laser at Saturation*, Phys. Rev. Lett. 88 (2002) 204801.

[5-45] W. Brefeld et al., *Scheme for time-resolved experiments based on the use of statistical properties of the third harmonic of the SASE FEL radiation*, Nucl. Instrum. and Methods A 507 (2003) 431.

[5-46] E.L. Saldin, E.A. Schneidmiller and M.V. Yurkov, *Properties of the Odd Harmonics of the Radiation from SASE FEL with a Planar Undulator*, Phys. Rev. ST 9(2006) 030702.

[5-47] G. Geloni, E.L. Saldin, E.A. Schneidmiller and M.V. Yurkov, *Exact Solution for the Second Harmonic Generation in XFELs*, DESY report 2005-137, DESY, Hamburg (2005).

[5-48] A.L. Cavalieri et al., *Clocking Femtosecond X-rays*, Phys. Rev. Lett. 94 (2005) 114801.

[5-49] A.M. Lindenberg et al., *Atomic-Scale Visualization of Inertial Dynamics*, Science 308 (2005) 392.

[5-50] T. Tanaka, H. Kitamura, *SPECTRA: a synchrotron radiation calculation code*, J. Synchrotron Rad. 8 (2001) 1221.

[5-51] P. Elleaume, J. Chavanne, B. Faatz, *Design considerations for an 1 Angstroem SASE undulator*, Nucl. Instrum. and Methods A 455 (2000) 503.

[5-52] K. Halbach, Nucl. Instrum. and Methods 187 (1987) 109.

[5-53] S. Sasaki, *Analyses for a planar variably-polarizing undulator*, Nucl. Instrum. and Methods A 347 (1994) 83.

[5-54] J. Chavanne and P. Elleaume, Synchrotron Radiation News 8 (1995) 18-22.

[5-55] I. Vasserman and E.R. Moog, *A passive scheme for ID end correction*, Rev. Sci. Instr. 66 (1995) 1943.

[5-56] J. Pflüger, H. Lu, T. Teichmann, *Field fine tuning by pole height adjustment for the undulator of the TTF–FEL,* Nucl. Instrum. and Methods A 429 (1999) 386.

[5-57] J. Pflüger, G. Heintze, I. Vasserman, *Search for possible radiation damage on a NdFeB permanent magnet structure after two years of operation*, Rev. Sci. Instr. 66 (1995) 1946.

Undulators for SASE and spontaneous emission – References

[5-58]   E. R. Moog, P. K. Den Hartog, E. J. Semones, P. K. Job, Proc. of the 10th National US conference on Synchrotron Radiation Instrumentation , CP417 (1997) 219.

[5-59]   J. Pflüger, B. Faatz, M. Tischer, T. Vielitz, *Radiation exposure and magnetic performance of the undulator system for the VUV FEL at the TESLA Test Facility Phase-1 after 3 years of operation*, Nucl. Instrum. and Methods A 507 (2003) 186.

[5-60]   S. Okuda, K. Okashi, N. Kobayashi, *Effects of electron-beam and ã-ray irradiation on the magnetic flux of Nd-Fe-B and Sm-Co permanent magnets*, Nucl. Instrum. and Methods B 94 (1994) 227.

[5-61]   H. Henschel, M. Körfer, K. Wittenburg, F. Wulf, *Fiberoptic radiation sensing system for TESLA*, TESLA report 2000-26, DESY, Hamburg (2000).

[5-62]   J. Pflüger, M. Tischer, *A Prototype Phase Shifter for the Undulator Systems at the TESLA X-ray FEL*, TESLA-FEL 2000-08 report, DESY, Hamburg (2000), http://tesla.desy.de/new_pages/0000_TESLA_Project.html

[5-63]   R. Tatchyn, *Selected applications of planar permanent magnet multipoles in FEL insertion device design*, Nucl. Instrum. and Methods A 341 (1994) 449.

[5-64]   J. Pflüger, Y. Nikitina, *Planar undulator schemes with strong focusing properties for the VUV-FEL at the TESLA test facility*, Nucl. Instr. and Methods A 381 (1996) 554.

[5-65]   J. Pflüger, H. Lu, D. Köster, T. Teichmann, *Magnetic measurements on the undulator prototype for the VUV-FEL at the TESLA Test Facility*, Nucl. Instrum. and Methods A 407 (1998) 386.

[5-66]   B. Faatz, *Beam Based Alignment of the TESLA X-Ray FEL Undulator*, TESLA-FEL report 1997-05, DESY, Hamburg (1997).

[5-67]   P. Castro, *TTF FEL Beam-based Alignment by Dispersion Correction Using Micado Algorithm*, TESLA-FEL report 1997-05, DESY, Hamburg (1997).

[5-68]   P. Emma, *Electron Phase Slip in an Undulator with Dipole Field and BPM Errors*, SLAC-TN-05-034, LCLS-TN-00-14, SLAC, Stanford (2000).

[5-69]   R. Treusch et al., *Development of photon beam diagnostics for VUV radiation from a SASE FEL*, Nucl. Instrum. and Methods A 445 (2000) 456.

[5-70]   K. Tiedtke et al., *The SASE FEL at DESY: Photon Beam Diagnostics for the User Facility*, Proceedings SRI2003, San Francisco, AIP Conf. Proc. 705 (2004) 588.

[5-71]   R. Treusch, *Photon Diagnostics for the VUV-FEL*, HASYLAB Annual Report 2005, DESY, Hamburg (2005) 159-164.

Undulators for SASE and spontaneous emission – References

[5-72] E. Gluskin et al., *The magnetic and diagnostic systems for the Advanced Photon Source self-amplified spontaneously emitting FEL*, Nucl. Instrum. and Methods A 429 (1999) 358.

[5-73] E. Gluskin, P. Illinski, N. Vinokurov, *Predicted performance of the LCLS X-ray diagnostics*, LCLS-TN-00-13, SLAC, Stanford (2000).

[5-74] B.X. Yang, *High resolution undulator measurements using angle-integrated spontaneous radiation*, Proceedings PAC05, Knoxville, Tennesse (2005).

[5-75] O. Chubar, P. Elleaume, SRW, Version 3.7, ESRF 1997–2000.

[5-76] B. Faatz, J. Pflüger, *Field Accuracy Requirements for the Undulator Systems of the X-Ray FEL's at TESLA*, TESLA-FEL report 2000-14, DESY, Hamburg (2000).

[5-77] B. Faatz, Private communication.

[5-78] U. Hahn, H. Schulte-Schrepping, *Emittance Measurements at the PETRA Undulator Beamline*, HASYLAB Jahresbericht 2001, DESY, Hamburg (2001) 105.

[5-79] U. Hahn, H. Schulte-Schrepping, *Crystal monochromator based emittance measurements at the PETRA undulator beamline*, SRI 2003 conference, San Francisco, AIP Conf. Proc. 705 (2003) 533.

[5-80] E.L. Saldin, E.A. Schneidmiller and M.V. Yurkov, *The Potential for the Development of the X-Ray Free Electron Laser*, TESLA-FEL report 2004-02, DESY, Hamburg (2004).

[5-81] J. Feldhaus et al., *Efficient frequency doubler for the soft X-ray SASE FEL at the TESLA Test Facility*, Nucl. Instrum. and Methods A 528 (2004) 471.

[5-82] E.L. Saldin, E.A. Schneidmiller and M.V. Yurkov, *Terawatt-scale sub-10-fs laser technology – key to generation of GW-level attosecond pulses in X-ray free electron laser*, Opt. Commun. 237 (2004) 153.

[5-83] E.L. Saldin, E.A. Schneidmiller and M.V. Yurkov, *A new technique to generate 100 GW-level attosecond X-ray pulses from the X-ray SASE FELs*, Opt. Commun. 239 (2004) 161.

[5-84] J. Feldhaus et al., *Possible application of X-ray optical elements for reducing the spectral bandwidth of an X-ray SASE FEL*, Opt. Commun. 140 (1997) 341.

[5-85] E.L. Saldin, E.A. Schneidmiller, Yu.V. Shvyd'ko and M.V. Yurkov, *X-ray FEL with a meV bandwidth, Nucl. Instrum. and Methods A 475 (2001) 357.*